MODELING THE EFFECT OF BINDING KINETICS IN SPATIAL DRUG DISTRIBUTION IN THE BRAIN

Nelson Kashaju

A Dissertation Submitted in Partial Fulfilment of the Requirements for the Degree of Masters in Mathematical and Computer Sciences and Engineering of the Nelson Mandela African Institution of Science and Technology

Arusha, Tanzania

August, 2021

ABSTRACT

Key factors in the process of drug delivery in the human brain are blood-brain barrier, drug distribution and drug binding kinetics. Since human brain is entirely unavailable for experimentation, mathematical models have become vital for improved visualization of how each of the key factors affects the delivery of drugs in the the human brain. In this study, a 3-dimensional mathematical model that incorporates drug transport across the blood-brain barrier, binding kinetics and drug distribution within the brain extracellular fluid with a bidirectional bulk flow of the brain extracellular fluid was developed and simulated. The model was developed assuming a cube volume of a brain unit that is a union of the blood-brain barrier, brain extracellular fluid and the blood plasma sub-domains. The model includes a set of partial differential equations and boundary conditions that characterize the processes in the specified sub-domains. To determine the effect of drug binding kinetics, the model equations together with their prescribed boundary conditions were discretized by employing the finite difference method implicit schemes and the model was analysed and simulated using MATLAB coding. Effects of drug binding kinetics were investigated by varying the binding parameter values for both specific and non-specific binding sites. All variations of binding parameter values were discussed and the results show the improved visualization of the effect of binding kinetics in drug distribution within the brain. For more realistic visualization, it was suggested to integrate more brain components that make up the large volume of the brain tissue.

DECLARATION

I, Nelson Kashaju, do hereby declare to the senate of Nelson Mandela African Institution of Science and Technology that this dissertation is my own original and it has neither been submitted nor presented for similar award in any other institution.

Nelson Kashaju		06-08-2021
Candidate Name	**Signature**	**Date**

The above declaration is confirmed by

Prof. Dr-Ing. Verdiana Grace Masanja		08-08-2021
Supervisor 1	**Signature**	**Date**

Dr. Mark Kimathi		06-08-2021
Supervisor 2	**Signature**	**Date**

COPYRIGHT

CERTIFICATION

The undersigned certify that they have read and hereby recommend for acceptance by the Nelson Mandela African Institution of Science and Technology the dissertation entitled: *Modeling the Effect of Binding Kinetics in Spatial Drug Distribution in the Brain*, in fulfilment of the requirements for the degree of Master's in Mathematical and Computer Science and Engineering of the Nelson Mandela African Institution of Science and Technology.

Prof. Dr-Ing. Verdiana Grace Masanja		08-08-2021
Supervisor 1	**Signature**	**Date**

Dr. Mark Kimathi		
Supervisor 2	**Signature**	**Date**

ACKNOWLEDGEMENTS

First and foremost, I would love to sincerely thank the Almighty God for his relentless protection, graces, and sustenance throughout the period of my study.

My heartfelt gratitude goes to my family, particularly my lovely mother Mrs. Salama Kashaju and beloved uncles Mr. Rweikiza Rwekamwa and Mr. Ludovick Kabelinde for always being there with great love, support and prayers throughout the time of my study.

I sincerely thank my supervisors, Prof. Verdiana G. Masanja and Dr. Mark Kimathi for their invaluable guidance and support in ensuring that this work is successfully accomplished.

Lastly, I would like to thank all my relatives, siblings, friends and colleagues for their relentless support throughout the period of my study.

DEDICATION

To my late father Mr. Ludovick Kashaju Bazigiza and my lovely mother Mrs. Salama Kashaju whose love, prayers and support have been so much helpful in every step of my life.

TABLE OF CONTENTS

LIST OF TABLES

LIST OF FIGURES

LIST OF APPENDICES

LIST OF ABBREVIATIONS AND SYMBOLS

BBB	Blood-Brain Barrier
BCECs	Brain Capillary Endothelial Cells
CSF	Cerebrospinal Fluid
DEs	Differential Equations
ECF	Extracellular Fluid
EEG	Electroencephalogram
FDM	Finite Difference Method

CHAPTER ONE

INTRODUCTION

1.1 Background of the Study

For many years, drug distribution for effective treatments within animal bodies has been a very challenging issue in the field of health sciences, specifically in pharmacological studies. The distribution of drug is simply a mechanism by which the drug compounds are distributed from the bloodstream to different body compartments, especially where their therapeutic effect is required (Paul, 2019; Vendel *et al.*, 2020). Once a drug is absorbed into the bloodstream, it is taken by the blood to different areas of the body which are organs and tissues. Drug distribution within animal bodies is a crucial process which results into exposing the targeted sites to the drug. Besides, drugs can only induce their therapeutic effects if they properly associate with the molecular targets within the body (Vendel *et al.*, 2020).

When the drug is administered into the brain, it is typically distributed variably due to various factors such as; blood perfusion, permeability of the blood-brain barrier (BBB), diffusion, the bulk flow of the brain extracellular fluid (ECF), metabolism and drug binding (Sim, 2015). Moreover, compounds of drug have the tendency of attaching themselves to their binding targets which are mainly the brain tissue components. Therefore, the drug concentration in the blood may considerably differ from that in the brain, also local differences in drug concentration-time profiles within the brain may grow. The local concentration-time profiles in the brain are very significant, as the effect of the drug is motored by the concentration–time profile at its binding sites. It is therefore necessary to consider the binding kinetics in drug distribution as this component describes the changes of concentration in a free drug and free binding targets in drug distribution process (Sykes *et al.*, 2019).

Blood separates from the brain by a semi-permeable border known as the BBB. The BBB is made of the endothelial cells situated in the brain that is made up of neighboring capillary cells. The narrow intercellular spaces of these cells tend to restrict the intercellular diffusion (Hladky & Barrand, 2016). Besides, molecular particles located in the endothelial capillary cells affect the drug transport across the BBB. These molecular particles move from the blood to the brain and vice-versa. Thus, drug concentration in the brain may significantly vary from concentration in the blood (Pardridge, 2016).

Drug compounds need to be passed on to specific targets in enough amounts and continuance so that they sufficiently act together with the binding targets and evoke the expected effect. As a result, numerical understanding is greatly needed on binding positions and binding kinetics in the brain for suitable prediction of a drug effect (Vendel *et al.*, 2019*b*). The human brain is solely unavailable for experiments. Moreover, the instant measuring of the distribution of the drug within the brain space is highly limited, as a result an extreme restriction is imposed on measuring concentration-time profile of a drug. In this particular case, a mathematical model becomes a very useful and facilitative tool for adequately forecasting the distribution of the drug in the brain and more significantly to depict and gain insights about the impact of processes that influence distribution of the drug, especially those that occur within the brain (Vendel *et al.*, 2019*b*).

Several studies on drug distribution within the brain have been recently conducted to study how different factors influence the prediction of drug distribution within the brain. A 2-dimensional mathematical model developed by Vendel *et al.* (2019*a*) was used to study the improved prediction of local drug distribution profiles within the brain. Furthermore, another 3-dimensional model by Vendel *et al.* (2020) was developed to further improve the prediction of drug distribution within the brain. Despite accommodating the key components involved in the drug distribution within the brain, both 2-dimensional and 3-dimensional models considered only one-direction of the bulk flow of the brain ECF leading to limited visualization of drug distribution within the brain.

Consequently, this study aim was to formulate a 3-dimensional mathematical model, to study the effect of the binding kinetics in the distribution of a drug when integrated with drug transport across the BBB and the distribution within the brain ECF while considering the bidirectional bulk flow of the brain ECF.

1.2 Statement of the Problem

When the drug is taken, either by injection or via other drug administration routes, its distribution in the brain involves a number of processes and factors such as the BBB, drug distribution, metabolism, bulk flow of the ECF, bulk flow of cerebrospinal fluid (CSF) as well as the drug binding kinetics. Out of the above outlined processes and factors, the key components involved in the distribution of drug in the brain are the BBB, drug distribution and the drug binding kinet-

ics. Because of the unavailability of the human brain for experimental purposes, and the current limits in the instant measuring of drug distribution in the brain space (Vendel *et al.*, 2019*b*), there was a need for a model which accommodates the BBB, drug distribution within the brain ECF, drug binding kinetics as well as the bidirectional bulk flow of the brain ECF.

Though current studies reveal that many models include the important factors affecting drug distribution within the brain, a very few of them explicitly describe drug binding kinetics and a few studies address the distinction between specific and non-specific binding (Vendel *et al.*, 2019*b*). The models take into account key processes of drug distribution, such as diffusion, the brain ECF bulk flow, and drug efflux to the brain capillaries and metabolism but, there is no model that integrates all these key components while considering a bidirectional bulk movement of the brain ECF. Moreover, there is no existing 3-dimensional model that simultaneously incorporates all the following key components i.e. the distribution across the BBB, the drug distribution within the brain and the drug binding kinetics taking into account the bidirectional bulk movement of the brain ECF.

It was thus deemed important to study the fate of a drug after it crosses the BBB, as many processes within the brain can affect the drug concentration and thereby influence its effect. As a result, this present study proposed a 3-dimensional model that integrates all the three components (distribution across the BBB, the binding kinetics, and the distribution within the brain ECF with a bidirectional bulk movement of the brain ECF) which are necessary for more accurate prediction of drug distribution within the brain.

1.3 Rationale of the Study

This study has provided useful information about drug distribution process in the brain, particularly the impact imposed on drug distribution by various factors involved in the whole process. The process is affected by several factors such as drug distribution in the brain ECF, binding kinetics, transport across the BBB, metabolism and bulk flow of the brain ECF. Limited knowledge on how the drug distributes within the brain poses a big challenge in accurately predicting the distribution of drug within the brain. Therefore, this study aimed to develop a model which will give improved visualization of how the drug distributes in the brain, thus rendering useful insights about drug distribution in the brain.

1.4 Research Objectives

1.4.1 General Objective

To study the effect of binding kinetics using a 3-dimensional mathematical model that incorporates the BBB, binding kinetics and drug distribution in the brain.

1.4.2 Specific Objectives

The specific objectives of this study are:

(i) To develop a 3-dimensional mathematical model that incorporates the BBB together with binding kinetics and drug distribution within the brain ECF.

(ii) To determine the effect of the integrated binding kinetics in predicting drug distribution in the brain.

1.5 Research Questions

The study is guided by the following questions:

(i) Can the Differential Equations (DEs) be used to adequately develop a 3-dimensional model that integrates the BBB, a bidirectional bulk movement of the brain ECF in drug distribution and the drug binding kinetics?

(ii) How significant is the influence of drug binding kinetics in the distribution of the drug in the brain?

1.6 Significance of the study

The results of this study put emphasis on the importance of drug bindings for improved predictions of drug concentration in drug distribution within the brain. Also, the results might help in giving light to pharmacologists and drug manufacturing industries on the impact of factors involved in drug distribution process. Last but not least, this study serves as a road map for further research in the pharmacology field.

1.7 Delineation of the Study

The study focused on drug distribution within the brain. In this study, the drug transport across the BBB, drug binding kinetics and the drug distribution in the brain ECF were considered as the key components involved in drug distribution. The formulated model of this study aimed at determining the effect of binding kinetics in drug distribution through integrating all the mentioned key components involved in drug distribution, while considering bidirectional bulk movement in the ECF.

CHAPTER TWO

LITERATURE REVIEW

2.1 Distribution of Drug within the Brain

Drug distribution process within human bodies, particularly in the brain is one of the major challenging issues in the field of pharmacology as it involves different complex components that govern the drug concentration-time profiles. The key complex components are such as; drug transport across the BBB, the distribution of the drug within the brain ECF as well as the binding kinetics of the drug (Vendel *et al.*, 2019*b*).

Since pharmacology field is one of the rapidly growing areas of interests for researchers, numerous studies have been conducted pertaining the drug distribution process within the brain which involves transport of drug across the BBB, distribution of drug within the brain ECF as well as the binding kinetics, also some models that describe the drug distribution process have been developed.

2.1.1 Transport of Drug across the Blood Brain Barrier

The transport of drug compounds from the blood into the brain is highly controlled by the semipermeable border of the brain known as the BBB whose main function is to split-up blood from the brain (Sweeney *et al.*, 2019). The BBB is made of the brain capillary endothelial cells (BCECs) that make up the brain capillaries. The BCECs make a co-operating complex with astrocytes and pericytes to serve a purpose of maintaining the brain homeostasis as well as selectively regulating the transport of nutrients and solutes carried by blood into the brain parenchyma. Also, the BCECs mostly depend on the intercellular interaction with the brain astrocytes and pericytes for its functions and maturation (Upadhyay, 2014).

For the BBB operating cells, the astrocytes are the glial family members that network with neurons and other cells of the brain like endothelial cells and microglia by either direct or indirect means or both via the exchange of soluble particles (Langhoff *et al.*, 2018). The astrocytes, also known as the supportive cells link with neurons and pericytes resulting into the formation of the neurovascular unit which is actually the barrier of the brain (Hawkins & Davis, 2005). Considering the nature of the drug, the transport of drug compounds may be more restricted or

less restricted to pass across the BBB. The multi-protein complexes called tight junctions are situated between the neighboring brain capillary endothelial cells that result into closing up the intercellular space, and therefore restricting the intercellular diffusion. Additionally, the ability of the drug to pass across the BBB largely depends on both the biological features such as transporters and enzymes, as well as the drug compounds physicochemical properties like molecular weight, lipophilicity and hydrogen bonding capacity (Barar *et al.*, 2016).

Nearly all drugs move into the brain from the blood after slipping through the BBB. The transport of drug compounds across the BBB may occur in two possible ways, which is either passive or active transport, and all these transport mechanisms demand different modeling approaches (Vendel *et al.*, 2019*b*). In 2014, an explanation for passive transport across the BBB was provided, that this transport aspect exhibits a bidirectional movement of drug compounds i.e. transport from the blood to the brain ECF and from the brain ECF to the blood. In this case the passive flux of drug through the BBB between the brain ECF and blood plasma is bidirectional and perpendicular to the BBB. Furthermore, it depends on the permeability of the BBB as well as the concentration change in the plasma of blood and brain ECF (Nhan *et al.*, 2014). However, an assumption is made that the width of the BBB tight junction is considered being equal to the diffusing drug through the BBB via the intercellular spaces for passive permeability in passive transport. Therefore, ignoring the tortuous shape of the BBB tight junctions result into underestimating the actual distance travelled by the diffusing drug (Nhan *et al.*, 2014).

Unlike the passive transport, active transport across the BBB exhibits the unidirectional movement of molecules from the blood to the brain. In this type of transport, the total flux in active transport across the BBB is as similarly described as in passive transport across the BBB and thus result into disregarding of unidirectional movement of molecules in the active transport across the BBB (Vendel *et al.*, 2019*b*). Moreover, the total flux of the drug active transport largely depends on the affinity of a drug for both, in and out of the brain (Yamamoto *et al.*, 2017). However, the active transport is generally assumed to function as stated by Michaelis-Menten kinetics (Syvänen *et al.*, 2006; Westerhout *et al.*, 2013, 2014). Since, the BBB acts as the main barrier of the brain that separates blood from the brain ECF, the drug concentration-time profile in the blood may significantly differ from that in the brain (Hladky & Barrand, 2016).

2.1.2 Drug Distribution within the Brain Extracellular Fluid

The drug within a brain is subjected to both drug diffusion into the brain ECF and bulk flow of the brain ECF after it passes across the BBB (Vendel *et al.*, 2020). In the brain ECF, drug diffusion is constrained by the obstruction imposed by the substances and/or cells found within the brain ECF which result into a phenomenon known as tortuosity (Syková & Nicholson, 2008). Tortuosity is a diffusion property whereby diffusion is hindered by factors such as spaces occupied by brain cells as well as extracellular matrix. Furthermore, this property differs for different drugs due to their differences in size, drug deformability as well as specific interactions of the drug with the extracellular matrix (Vendel *et al.*, 2019*b*).

In the year 1956, Einstein provided an equation that he used to describe molecular movement in liquid medium, in line with that, the equation is commonly used in various models to describe the movement of a compound through a medium like the brain ECF by diffusion process (Einstein, 1905). Since the brain ECF has a complex structure, it turns-out that the diffusion of drug molecules via the brain ECF is lessened due to various factors like the hindrance imposed by the brain cells (tortuosity) and volume fraction of the brain ECF. Hence this leads to the situation whereby the effective diffusion within the brain ECF becomes different from the one in a normal medium such as water. However, in 2019 Vendel suggested that in order to account for the complex intertwined structure of the brain, the diffusion equation needs to further be fine-tuned through taking into account the tortuosity and the brain ECF volume fraction (Vendel *et al.*, 2019*a*).

In spite of all the massive work that has been done on modeling the diffusion of drug molecules through the brain ECF, the most recent study done in 2020 by Lange reveals that in a 3-dimensional brain unit only a one dimensional bulk flow of the brain ECF is assumed which limits the visualization of the drug bound to either specific or non-specific binding targets. As a result, the mentioned situation demands a 3-dimensional model with at least two-dimensional bulk flow of the brain ECF (Vendel *et al.*, 2020).

2.1.3 Drug Binding Kinetics

The binding of drug compounds to either specific or non-specific targets is one of the key determinants of the effect induced to the body by the drug. It basically refers to how speedy the drug compounds associate with its targeted sites as well as how it dissociates from it. Thus,

this phenomenon is in fact concerned with measuring of two kinds of rates; the on-rate and the off-rate (Clarelli *et al.*, 2020).

Although drug binding kinetics is an essential component in the entire process of drug distribution; this component has not been significantly considered in some studies due to different reasons. Piet van der Graaf, a systems biology professor from University of Leiden claims that measuring the on-rate/off-rate used to be a torturous and long process (Owens, 2007). This is the reason why up to the early of 21st century, most pharmaceutical companies could not screen for the on-rate and off-rate due to the lengthy and expensive screening process. This situation triggered different modeling approaches to study how binding kinetics of the drug influences drug effect in its binding sites (Owens, 2007).

In 2017, a study was conducted on the influence of drug distribution and drug-target binding on target occupancy. The study used the steady-state approximation and rate-limiting step approximation approaches to investigate the influence of binding kinetics of the target of drug. The study revealed that even though both approaches demonstrate the significance of high target concentration and drug rate of association on the binding sites, the rate-limiting approximation is more accurate compared to steady-state approximation specifically when the dissociation rate is faster than association rate (de Witte *et al.*, 2017).

In 2018, another study was done concerning modeling the delay between pharmacokinetics and electroencephalogram (EEG) effects of morphine in rats, comparing binding kinetics and compartment models. The study aimed at exploring when to use the drug-target binding model instead of the effect compartment model through testing the usefulness of three different models; the effect compartment, target-binding kinetics as well as the combined effect compartment-target binding kinetics models. The test on all these models was done particularly on plasma, and/or brain extracellular fluid morphine concentrations and EEG amplitude in rats. Although all three models performed the same in describing the morphine pharmacodynamics, the effect compartment model provided the best statistical result. Additionally, the study claims that, since the target binding model can be learned via in vitro measurements of the rates of association and dissociation, a target binding model should then be more often taken into account for aiding mechanistic modeling (de Witte *et al.*, 2018).

2.2 Research Gap

Although many studies have been conducted in the recent years regarding the distribution of drug within the brain, much is still uncovered concerning the effect of drug binding kinetics within the brain. Moreover, the current 2-dimensional models for drug distribution within the brain don't adequately describe the effect of drug binding kinetics. Also, the currently available 3-dimensional models have a unidirectional bulk flow of the brain ECF. This therefore called for developing a 3-dimensional model with a bidirectional bulk flow of the brain ECF that has provided improved visualization of drug concentrations. This has also assisted in gaining more insights about how the drug passes on into and within the brain so as to further enhance the adequate prediction of the effect of a drug that binds to both specific and non-specific binding targets.

CHAPTER THREE

MATERIALS AND METHODS

3.1 Study Area and Scope of the Research

For many years, drug distribution for effective treatments within animal bodies has been a very challenging issue in the field of health sciences, particularly in pharmacology. Consequently, this challenge leads to the difficulties in developing drugs that bind to the targeted sites, especially in the brain.

There is a great demand of the significant knowledge about key components or processes involved in drug distribution process, especially the ones that control the concentration-time profiles of a drug within the brain. Some studies have been conducted on the processes that affect the drug distribution process in the brain. They include studies concerning drug transport across the BBB, bulk flow of the brain ECF, drug diffusion through the brain ECF, extra-intracellular exchange as well as bulk flow of CSF. However, there are few studies that explicitly describe the effect of binding kinetics when incorporated with other key components (Vendel *et al.*, 2019*b*). Moreover, the most recent 3D model limits the visualization due to the fact that it only considers one dimensional bulk flow of the brain's ECF (Vendel *et al.*, 2019*b*).

This study aim was to develop a new model for a 3-dimensional brain tissue unit that incorporates the drug transport across the BBB, drug transport in the brain ECF and the binding kinetics of the drug. Moreover, the model took into account the two-dimensional bulk flow of the brain ECF to lead to the improved visualization of local drug distribution in the brain.

3.2 Data Collection Methods

Secondary data were collected from different literature from which a range of parameter values of the model are found. However, the kinetic parameters pertaining to non-specific binding i.e. B_2^{tot}, k_{2on} and k_{2off} are chosen on the basis of an assumption that drug binding to specific binding sites is stronger than drug binding to non-specific binding sites.

3.3 Model Development

3.3.1 Model Assumptions

The model was developed on the basis of the following assumptions:

(i) The concentration of drug in the plasma of blood is defined as a function of both absorption rate and elimination rate into and from the blood plasma. In this case, the drug is assumed to be orally administered into the body.

(ii) The drug is carried into 3-dimensional brain unit by a supplying arteriole and exits via a draining venule, see Fig. 1(a).

(iii) The drug goes into the brain unit in the domain W_{in} and exits in the domain W_{out}, see Fig. 1(b).

(iv) The blood flow in brain capillaries is directed away from W_{in}.

(v) Diffusion within the blood plasma is negligible compared to the brain capillary blood flow hence drug is transported entirely through the brain capillaries by the brain capillary blood flow.

(vi) The brain capillaries are all equal in size and surface area. Additionally, it was further assumed that the volume of the incoming arteriole is the same as the volume of the three outgoing brain capillaries it links to and that the volume of the outgoing venule equals the volume of the three incoming brain capillaries it links to. As a result, the total volume of incoming blood conduits equals the total volume of the outgoing blood conduits at each vertex, while the brain capillary blood flow velocity is by default equal in all brain capillaries.

(vii) The whole drug within the blood plasma is in an unbound state, thus it can pass across the BBB. Furthermore, the exchange of drug between the blood plasma and the brain ECF is depicted through both passive and active transport across the BBB in both directions.

(viii) Drug within the brain ECF is transported by both diffusion and the brain ECF bulk flow.

(ix) Tortuosity is taken into consideration in order to account for the hindrance on diffusion imposed by the brain cells.

(x) Rectangular cartesian coordinate system is used to indicate the direction of the brain ECF bulk flow. The brain ECF bulk flow is bidirectional. It is directed in the x-direction and z-direction, see Fig. 1(c). Additionally, both the x-directed and z-directed bulk flows of the brain ECF are assumed to be the same.

(xi) The whole drug is distributed within the brain ECF and available at the extracellular binding sites.

(xii) The drug binding is reversible in such a way that total concentration of a drug in specific and non-specific binding sites is constant.

(xiii) The specific and non-specific targets are evenly distributed over a 3-dimensional brain unit and fixed.

(xiv) The specific and non-specific binding sites lie on the outside of cells and the drug does not have to cross cell membranes in order to bind to the binding sites.

The above assumptions were made to indicate properties of the human brain, drug-related properties as well as the processes involved in drug distribution within the brain (Vendel *et al.*, 2020).

Consider the following figures for reference;

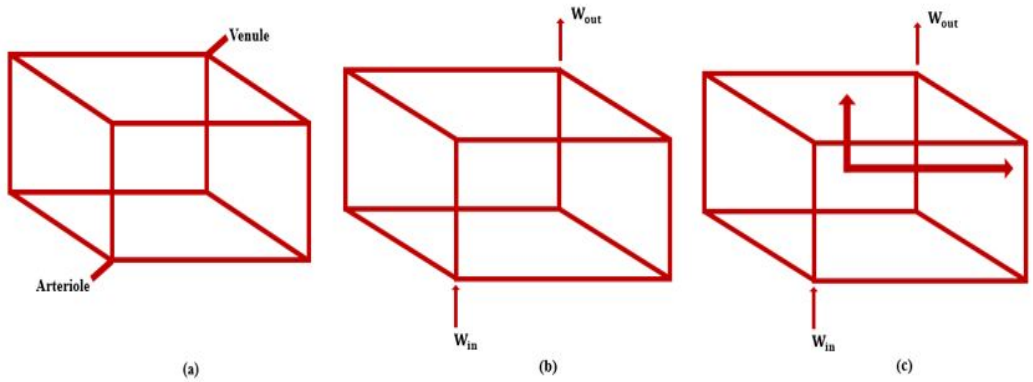

Figure 1: 3-dimensional Brain unit domain, indicating W_{in}, W_{out} domains and bulk flow directions

3.3.2 Description of 3 Dimensional Brain Unit

The model developed in this work considered a 3-dimensional brain unit as its domain, which is defined as:

$$W = \{(W_{xi}, W_{yi}, W_{zi}) \in \mathbb{R}^3 | 0 \leq \mathrm{W_{xi}} \leq \mathrm{x_r} \wedge 0 \leq \mathrm{W_{yi}} \leq \mathrm{y_r} \wedge 0 \leq \mathrm{W_{zi}} \leq \mathrm{z_r}\} \tag{1}$$

Whereby x_r, y_r and z_r stand for the length of one unit of the brain capillary, given by $l_{cap} + 2r$ with l_{cap} as the inter-capillary distance and r is the radius of brain capillary. Additionally, x-directed, y-directed and z-directed brain capillaries are the sets defined as $\{W_{xi},\ i = 1, ..., 4\}$, $\{W_{yi},\ i = 1, ..., 4\}$ and $\{W_{zi},\ i = 1, ..., 4\}$ respectively.

Since the brain capillaries, BBB, and ECF are found in the brain then they are the subsets of one unit of the brain (Vendel *et al.*, 2020). That is, $W_{pl} \subset W$, $W_{BBB} \subset W$and $W_{ECF} \subset W$. Therefore, the domain of a 3-dimensional brain unit can be defined as:

$$W = W_{pl} \cup W_{BBB} \cup W_{ECF} \tag{2}$$

3.3.3 Demonstration of Drug Distribution in Blood Plasma Domain, W_{pl}

According to assumption 3.3.2(i)., the drug is assumed to be orally administered. Thus, the concentration of unbound drug within W_{pl} is expressed by the Equation 3:

$$\mu(t)_{W_{in}} = \frac{F.Dose.K_a}{V_d(K_a - K_e)}(e^{-K_e t} - e^{-K_a t}) \tag{3}$$

Whereby, F is the drug bioavailability, μ is the drug concentration within the blood plasma, $Dose$ is the orally delivered drug concentration, V_d is the distribution volume that relates the drug concentration in the blood plasma with the total drug amount in the body , K_a and K_e are the drug absorption and elimination constants respectively.

Moreover, according to assumptions 3.3.2(iv) and 3.3.2(v), the Equations governing the motion of drug concentration in blood plasma reduce to Equations 4:

$$\begin{aligned}
\frac{\partial \mu}{\partial t} &= -v_{blood}\frac{\partial \mu}{\partial x}, \mu \in W_{xi}, \forall_i | i = 1, ..., 4. \\
\frac{\partial \mu}{\partial t} &= -v_{blood}\frac{\partial \mu}{\partial y}, \mu \in W_{yi}, \forall_i | i = 1, ..., 4. \\
\frac{\partial \mu}{\partial t} &= -v_{blood}\frac{\partial \mu}{\partial z}, \mu \in W_{zi}, \forall_i | i = 1, ..., 4.
\end{aligned} \tag{4}$$

The associated initial condition is:

$$\mu(x, y, z, t = 0) = 0 \tag{5}$$

Where, v_{blood} is the blood flow velocity in the brain capillaries. W_{xi}, W_{yi} and W_{zi}, $\forall_i | i = 1, ..., 4$ represent the directions of brain capillaries in x, y and z direction respectively.

3.3.4 Description of Drug Distribution in Brain ECF Domain, W_{ECF}

Also, based on assumptions 3.3.2(viii) to 3.3.2(xiv), the distribution of both bound and unbound drug within W_{ECF} is described by the Equations 6, 7 and 8:

$$\frac{\partial \rho}{\partial t} = \frac{D}{\lambda^2}\nabla^2\rho - v_{ECF}(\frac{\partial \rho}{\partial x} + \frac{\partial \rho}{\partial z}) - k_{1on}\rho(B_1^{tot} - B_1) + k_{1off}B_1 - k_{2on}\rho(B_2^{tot} - B_2) + K_{2off}B_2 \tag{6}$$

$$\frac{\partial B_1}{\partial t} = k_{1on}\rho(B_1^{tot} - B_1) - k_{1off}B_1 \tag{7}$$

$$\frac{\partial B_2}{\partial t} = k_{2on}\rho(B_2^{tot} - B_2) - K_{2off}B_2 \tag{8}$$

The associated initial conditions are:

$$\rho(x, y, z, t = 0) = 0 \tag{9}$$

And;

$$B_i(x, y, z, t = 0) = 0, \ \forall_i | i = 1, 2 \tag{10}$$

Whereby, D is the diffusion coefficient in a free medium, λ is the tortuosity, ρ is the concentration of drug in the brain ECF, v_{ECF} is the (x-directed and z-directed) brain ECF bulk flow (Vendel *et al.*, 2019*b*). Furthermore, B_1 and B_2 are the concentrations of drug bound to both specific binding and non-specific binding sites respectively, B_1^{tot} and B_2^{tot} are the total concentrations of specific binding and non-specific binding sites within the brain ECF respectively (Vendel *et al.*, 2019*a*). Also, k_{1on} and k_{2on} are the association rate constant for both specific binding and non-specific binding respectively. Where, k_{1off} and k_{2off} are the dissociation rate constant for both specific and non-specific binding respectively (Vendel *et al.*, 2019*a*).

3.3.5 Boundary Conditions

The system of Equations 3, 4, 6, 7 and 8 along with their associated initial conditions 5, 9 and 10 form a mathematical model for this study. All of these Equations describe the process of drug distribution over different subdomains within a 3-dimensional brain unit domain.

In order to adequately solve the model Equations, it is important to specify realistic boundary conditions for this model. The boundaries are; the faces of the brain unit, the interface between the brain capillaries domain (W_{pl}) and the brain ECF domain (W_{ECF}) i.e. at $x = r$ and $x = x_r - r$ (see Fig. 2).

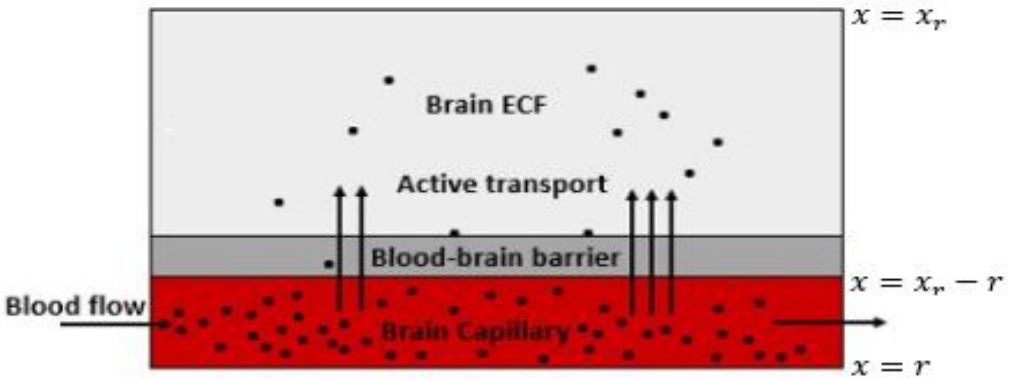

Figure 2: Drug exchange between W_{pl} and W_{ECF}

(i) **Drug exchange between W_{pl} and W_{ECF}**

The diffusion of a drug from the blood plasma into the brain ECF is described as a product of the difference in concentration of drug between W_{pl} and W_{ECF} $(\mu - \rho)$, and the BBB permeability (P). Moreover, the active transport into and out of the brain ECF is modeled through Michaelis-Menten Kinetics (Syvänen *et al.*, 2006; Bickel, 2005; Westerhout *et al.*, 2013, 2014)

Thus, based on (Vendel *et al.*, 2020), drug transport in and out of the brain is described by Equation 11:

$$f(\mu, \rho) = P(\mu - \rho) + \frac{T_{m-in}}{SA_{BBB}(K_{m-in} + \mu)}\mu - \frac{T_{m-out}}{SA_{BBB}(K_{m-out} + \rho)}\rho \tag{11}$$

With; $P = p_{trans}f_{trans} + p_{para}f_{para}$ where $p_{para} = \dfrac{D_{para}}{W_{PCS}}$

Where, p_{trans} is the permeability across the endothelial cells of brain capillary, f_{trans} is the fraction of the area of endothelial cells of brain capillary, D_{para} is the diffusivity of a drug across the paracellular space, W_{PCS} is the breadth of the paracellular space, f_{para} is the fraction of area of the paracellular space, the maximal rates of active influx and active efflux of drug are given by T_{m-in} and T_{m-out} respectively, K_{m-in} is the concentration of drug where half of

T_{m-in} is attained, K_{m-out} is the concentration of drug where half of T_{m-out} is attained and SA_{BBB} represents the surface area of the BBB (Vendel *et al.*, 2020).

As Fig. 2 indicates, the loss or gain of unbound drug from/into the brain ECF due to the BBB is described by the boundary conditions given by Equation 12 (Vendel *et al.*, 2019*a*):

$$\begin{aligned} D^* \frac{\partial \rho}{\partial t} &= -f(\mu, \rho)\ for\ (x, y, z) \in W_{BBB}\ at\ x = r \\ D^* \frac{\partial \rho}{\partial t} &= f(\mu, \rho)\ for\ (x, y, z) \in W_{BBB}\ at\ x = x_r - r \end{aligned} \tag{12}$$

Moreover, in view of the brain capillaries domain, the drug transport across the BBB is described by Equation 13:

$$\begin{aligned} D^* \frac{\partial \mu}{\partial t} &= f(\mu, \rho)\ for\ (x, y, z) \in W_{BBB}\ at\ x = r \\ D^* \frac{\partial \mu}{\partial t} &= -f(\mu, \rho)\ for\ (x, y, z) \in W_{BBB}\ at\ x = x_r - r \end{aligned} \tag{13}$$

Where $D^* = \dfrac{D}{\lambda^2}$, D^* is effective diffusion coefficient while D is the coefficient of diffusion in free medium.

Additionally, considering assumption 3.3.2(v) i.e. there's no diffusion in blood plasma. It follows that, the system of Equation 14 is used for description of the concentrations at the sides of 3-dimensional brain unit:

$$\begin{aligned} \frac{\partial \mu}{\partial x} &= 0\ for\ x = 0\ and\ x = x_r \\ \frac{\partial \mu}{\partial y} &= 0\ for\ y = 0\ and\ y = y_r \\ \frac{\partial \mu}{\partial z} &= 0\ for\ x = 0\ and\ z = z_r \end{aligned} \tag{14}$$

Following (Vendel *et al.*, 2020), in this study, the concentration is considered to be zero at the faces of a 3D brain unit, as given by the Equation 15:

$$\mu = 0\ for\ W_{out} \cap \partial W \tag{15}$$

Furthermore, the conditions at boundaries ($W_{ECF} \cap \partial W$) are given by Equation 16:

$$\frac{\partial \rho}{\partial x} = 0$$

$$\frac{\partial \rho}{\partial z} = 0 \tag{16}$$

3.4 Description of Model Parameters

In the current study, properties of the rat brain were used to determine the parameter values. This choice is made on the basis that most data for this species are available. Nevertheless, the model is suitably valid for data from human and other species. The brain inter-capillary distance in the rat is averagely considered to be $50\mu m$, whereby the brain capillary is approximately $2.5\mu m$ by radius (Tata & Anderson, 2002). It follows that, the radius of capillaries in the brain, r, was set to $2.5\mu m$ and the dimensions of the 3-dimensional brain unit in the directions of x,y and z to $55\mu m$.

Additionally, Equations 4 and 5 are used to describe concentration of the drug in blood plasma and the associated boundary conditions are described by Equations 13, 14 and 15. We also describe the concentration of drug within the brain ECF through Equations 6, 7 and 8, the initial conditions 9 and 10 along with boundary conditions described in Equations 12 and 16. The parameter values together with their units are given in Table 3.1. The choice of values for model parameters is based on the findings of different experimental studies while the assumed parameter values were estimated for numerical simulation purpose.

Table 3.1: The Model Parameters, Descriptions, Values, and Units

Parameter	Description	Value[Reference]	Unit
F	Drug bioavailability	1 (Vendel *et al.*, 2020)	-
$Dose$	Concentration of orally		
	delivered drug	0.5 (Tasso *et al.*, 2008)	μmol
V_d	Distribution volume	0.2 (Tasso *et al.*, 2008)	L
K_a	Absorption rate constant	$2 * 10^{-4}$ (Ball *et al.*, 2014)	s^{-1}
K_e	Elimination rate constant	$5 * 10^{-5}$ (Tasso *et al.*, 2008)	s^{-1}
r	Brain capillary radius	$2.5 * 10^{-6}$ (Karbowski, 2011)	m
l_{cap}	Inter-capillary distance	$5 * 10^{-5}$ (Reichel, 2015)	m
v_{blood}	Brain capillary blood		
	flow rate	$(0.5 - 50) * 10^{-6}$ (Reichel, 2015)	ms^{-1}
T_{m-in}	maximum active influx rate	$0.1 * 10^{-12}$(Assumed)	$\mu mols^{-1}$
T_{m-out}	maximum active efflux rate	$0.1 * 10^{-12}$(Assumed)	$\mu mols^{-1}$
K_{m-in}	Concentration required		
	to attain half of T_{m-in}	$1 * 10^{2}$ (Vendel *et al.*, 2020)	$\mu molL^{-1}$
K_{m-out}	Concentration required		
	to attain half of T_{m-in}	$1 * 10^{2}$ (Vendel *et al.*, 2020)	$\mu molL^{-1}$
D^*	Effective diffusion	$2.5 * 10^{-16}$ (Nicholson *et al.*, 2000)	m^2s^{-1}
V_{ECF}	Brain ECF bulk flow velocity	$0.5 * 10^{-6}$ (Vendel *et al.*, 2020)	ms^{-1}
SA_{BBB}	Surface area of the BBB	$0.1 * 10^{-7}$(Assumed)	m^2
P	BBB permeability	$10^{-10} - 10^{-5}$ (Wong *et al.*, 2013)	ms^{-1}
k_{1on}	Specific association		
	rate constant	$10^{-4} - 10^{2}$ (de Witte *et al.*, 2016)	$(\mu molL^{-1}s)^{-1}$
k_{2on}	Non-specific association		
	rate constant	$10^{-6} - 10^{1}$ (Vendel *et al.*, 2019*a*)	$(\mu molL^{-1}s)^{-1}$
k_{1off}	Specific dissociation		
	rate constant	$10^{-6} - 10^{1}$ (de Witte *et al.*, 2016)	s^{-1}
k_{2off}	Non-specific dissociation		
	rate constant	$10^{-4} - 10^{3}$ (Vendel *et al.*, 2019*a*)	s^{-1}
B_1^{tot}	Total concentration		
	on specific binding sites	$5 * 10^{-2}$ (de Witte *et al.*, 2016)	$\mu molL^{-1}$
B_2^{tot}	Total concentration		
	on non-specific binding sites	$5 * 10^{1}$ (Vendel *et al.*, 2019*a*)	$\mu molL^{-1}$

CHAPTER FOUR

RESULTS AND DISCUSSION

4.1 Model Results

Drug distribution in the 3-dimensional brain unit is studied by plotting the concentration of drug in the blood plasma, drug binding sites as well as the brain extracellular fluid for various time instances. The main focus of the current study is to determine the effect that the binding kinetics of drug imposes on the distribution of drug in the brain tissue. To determine the effect of drug binding kinetics, the model Equations 4, 6, 7 and 8 are discretized together with the prescribed boundary conditions 12, 13, 14 and 16. The discretization is done by using finite difference method (FDM), particularly the implicit schemes through which the simulation is carried out. For improved visualization of the effect of drug binding kinetics, drug distribution incorporated with drug transport across the BBB, binding kinetics of drug and bidirectional bulk flow of the brain ECF are considered. The parameter values in Table 3.1 are used for simulation.

The blood flow within brain capillaries aids the movement of drug compounds within a 3-dimensional brain unit. The drug compounds within blood plasma have to cross the BBB for them to enter the brain ECF. The drug compounds bind either to non-specific or specific binding targets in the brain ECF. In addition, the effect of binding kinetics is determined by studying the trends of how the drug distributes in the brain ECF. The drug transport process within the brain unit is described by Fig. 3(a). Moreover, the cubical lattice (blue) in Fig. 3(b) represents a piece of 3-dimensional brain tissue within which the brain ECF is found. The cubical lattice is formed of the network of smaller cubic lattices (red). The arrows indicate the bidirectional bulk flow of the brain ECF. In the simulations of the current study on how the drug distributes within the brain ECF, the cubical lattice in Fig. 3(b) is sliced at different positions into three slices plots such that the effect of binding kinetics and concentration within the brain ECF can be easily observed at different time levels.

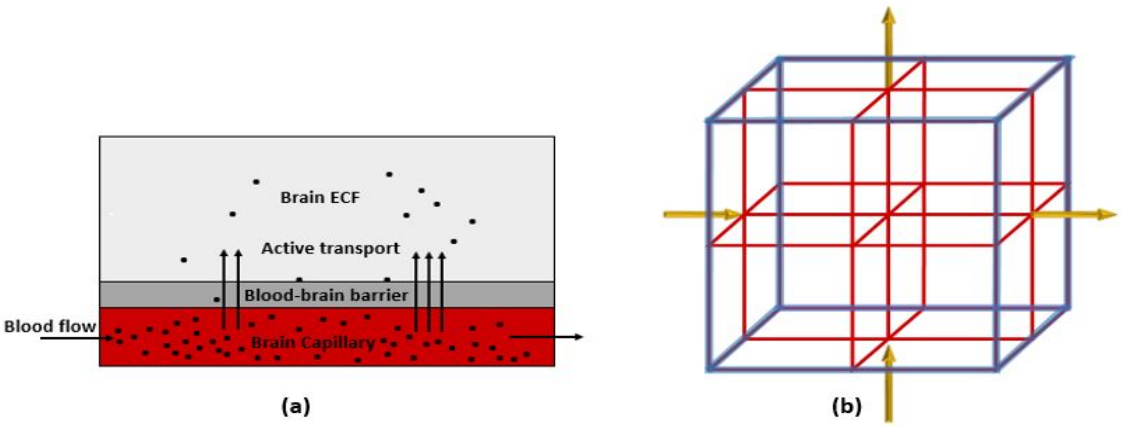

Figure 3: Drug transport in brain capillaries, active transport across the BBB into the brain ECF

4.1.1 Drug Distribution in Blood Plasma

The unbound compounds of the drug in the plasma have to pass through the BBB into the brain ECF where its therapeutic effect is determined. Determining how the drug concentration distributes along the brain capillaries across the BBB into the brain ECF is firstly done. The distribution is observed at three different levels of time $t_1 = 2sec$, $t_2 = 8sec$, and $t_3 = 14sec$. Drug compounds leave the blood plasma domain across the BBB into the brain ECF where the drug compounds bind to either binding or non-binding sites. The amount of unbound drug from blood plasma into the brain ECF is slightly affected by the permeability of BBB, P and blood flow rate, v_{blood}. Figures 4 - 7 show how the drug compounds distribute in the blood plasma when different cases of variations in the blood flow rate, v_{blood} and permeability of BBB, P are considered. The model parameter values for permeability $(P = 0.1 * 10^{-7} ms^{-1})$ and blood flow rate $(v_{blood} = 1 * 10^{-6} ms^{-1})$ are initially used in the simulations for Fig. 4 to describe how the drug distributes along brain capillaries into the brain ECF.

The plots in Fig. 4 show that, the concentration of drug within blood plasma slightly distributes within brain capillaries in significantly smaller amounts at different time levels for the mentioned permeability and blood flow velocity values. However, in Fig. 5 the concentration of unbound drug within blood plasma appears to become considerably large when the BBB permeability and blood rate values are simultaneously increased i.e. $(P = 0.5 * 10^{-7} ms^{-1})$ and $(v_{blood} = 1.5 * 10^{-6} ms^{-1})$. This implies that, when the values for both BBB permeability and blood flow rate are increased simultaneously, the compounds of unbound drug within the blood

plasma are found to have huge amount as seen in Fig. 5(a). However, as time passes, the drug distributes further and the concentration within the blood plasma becomes much more lesser due to elimination to the brain ECF. Thus, the concentration of drug within blood plasma tend to decrease as shown in Fig. 5(b) and (c). Moreover, in Fig. 5 when the BBB permeability (P) and blood flow rate (v_{blood}) are simultaneously increased, the concentration of unbound drug in blood plasma is as much as a square of the concentration of drug in blood plasma for smaller values of BBB permeability (P) and blood flow rate (v_{blood}) in Fig. 4.

Nevertheless, the plots in Fig. 4 exhibits spatial variations in the location of the drug concentration peaks in distribution of drug within the blood plasma at three different time levels. The variation of drug concentration peak within the blood plasma is initially observed at $t_1 = 2sec$ as indicated in Fig. 4(a). The concentration peak in Fig. 4(a) covers a small area contrary to Fig. 4(b) and (c). When the time increases to $t_2 = 8sec$, the concentration peak also spreads a little wider as shown in Fig. 4(b). Additionally, when the time increases further to $t_3 = 14sec$, the concentration peak within the blood plasma spread more over the region next to the BBB as indicated in Fig. 4(c).

Further, determining how the variations in individual parameter values of the BBB permeability (P) and blood flow rate (v_{blood}) respectively affect the distribution of drug within the blood plasma is done. The variation is done in one parameter value while the other parameter value is kept constant as shown in Fig. 6 and Fig. 7. Initially, the value for BBB permeability (P) is set to $P = 2 * 10^{-6.9} ms^{-1}$ while the blood flow rate is held constant, $v_{blood} = 1 * 10^{-6} ms^{-1}$. Thereafter, the blood flow rate is varied to $v_{blood} = 1.1 * 10^{-5.95} ms^{-1}$ while the BBB permeability is held constant, $P = 0.1 * 10^{-7} ms^{-1}$.

When the BBB permeability increases while blood flow rate is held constant, the concentration of unbound drug becomes less in the blood plasma. The Fig. 6 shows that, drug concentration within the blood plasma is slightly distributed in small amounts. Nevertheless, in a case when the blood flow rate is increased while the BBB permeability is held constant, an increased drug concentration within the blood plasma is observed as shown in Fig. 7. Moreover, spatial variations in drug concentration peak in Fig. 6 and Fig. 7 are observed at different time levels. In Fig. 6(a) and (b), the drug distribution within the blood plasma is approximately the same for the first two time levels i.e $t_1 = 2sec$ and $t_2 = 8sec$, however, the distribution of drug tend to increase in the region next to the BBB as time increases due to the increased permeability as

shown in Fig. 6(c). Additionally, in Fig. 7(a) the drug distribution within the blood plasma is observed to be less compared to that observed in Fig. 7(b), but as time goes on, the drug distribution in the blood plasma tends to decrease to a minimal drug concentration due to elimination of drug from the blood plasma, Fig. 7(c). The plots (a), (b) and (c) in Fig. 4 - 7 indicate the distribution of drug in the blood plasma (μ) for $t = 2s, t = 8s$ and $t = 14s$ respectively.

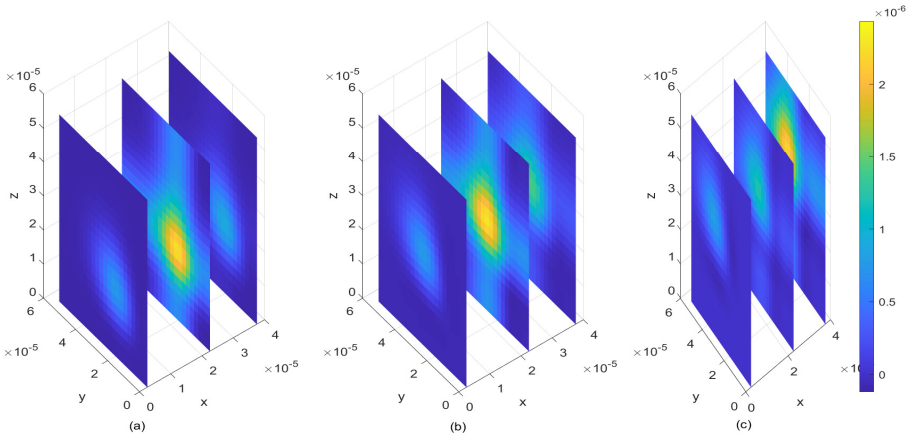

Figure 4: Drug distribution in blood plasma (μ) for $P = 0.1 * 10^{-7} ms^{-1}$ and v_{blood}=$1 * 10^{-6} ms^{-1}$

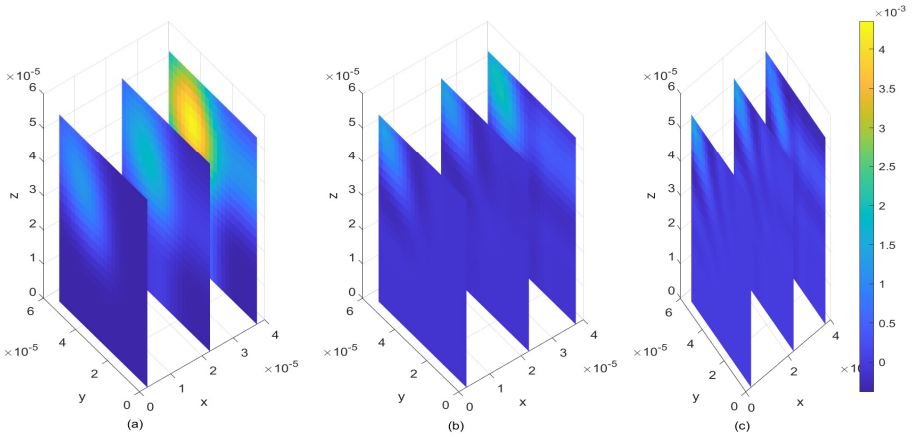

Figure 5: Drug distribution in blood plasma (μ) for Drug distribution in blood plasma (μ) for $P = 0.5 * 10^{-7} ms^{-1}$ and v_{blood}=$1.5 * 10^{-6} ms^{-1}$

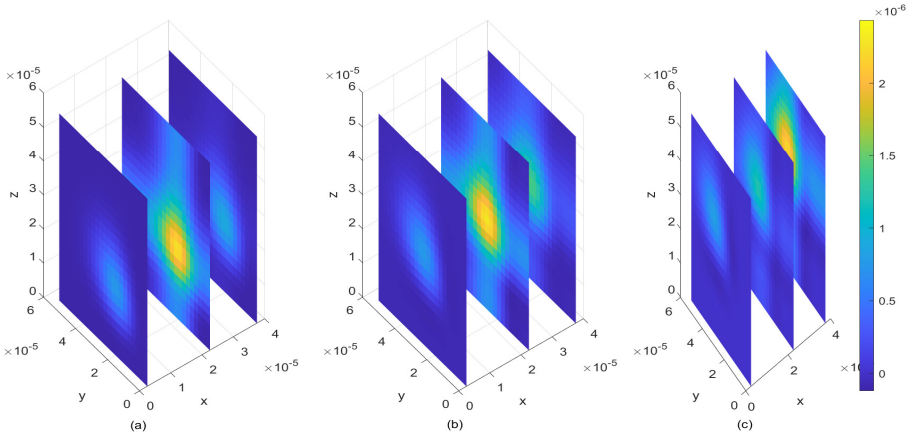

Figure 6: Drug distribution in blood plasma (μ) for Drug distribution in blood plasma (μ) for $P = 2 * 10^{-6.9} ms^{-1}$ and v_{blood}=$1 * 10^{-6} ms^{-1}$

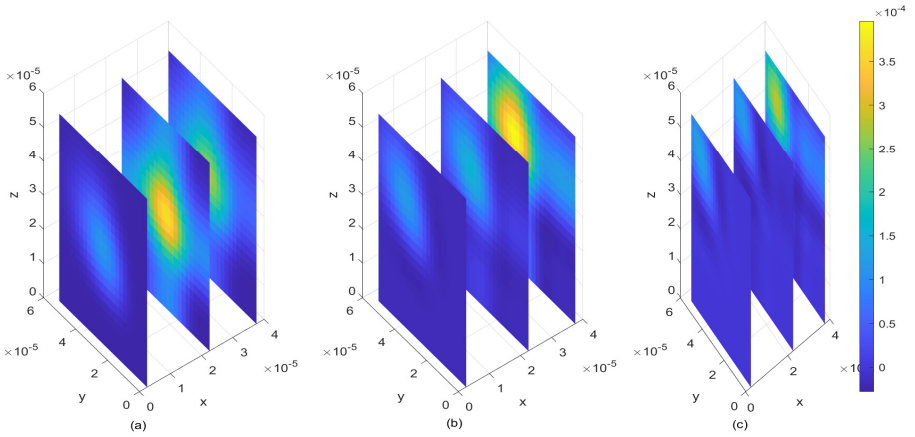

Figure 7: Drug distribution in blood plasma (μ) for Drug distribution in blood plasma (μ) for $P = 0.1 * 10^{-7} ms^{-1}$ and v_{blood}=$1.1 * 10^{-5.95} ms^{-1}$

4.1.2 The Effect of Binding Kinetics in Drug Distribution within a 3 Dimensional Brain Unit

After crossing the BBB, the drug compounds diffuse into the brain inter-cellular spaces and distribute throughout the brain ECF via the bulk flow of the brain ECF. However, the distribution of free drug compounds in the brain ECF is somewhat affected by the binding kinetics of the drug at their binding targets. Therefore, it's important to determine how the binding kinetics of drug affect the drug distribution within the brain.

Both diffusion and bulk flow of a drug result into a substantial amount of drug concentration within the brain ECF. This maximizes the chances of drug compounds to associate with either

specific or non-specific binding targets. Moreover, the chance for drug binding kinetics to induce its effect on drug distribution within the brain ECF becomes higher.

The impact of drug binding kinetics is determined through investigating the trends of distribution of a free drug within the brain ECF at three distinct time levels ($t_1 = 2sec$, $t_2 = 8sec$ and $t_3 = 14sec$) when different values for drug association and dissociation rates (k_{ion} and k_{ioff} respectively,for $i = 1, 2$) are considered in the simulated plots (see Fig. 8, 11, 14, 17 and 20).

First, a case whereby the model is simulated by fixed parameter values of binding kinetics to see how the drug distributes within the brain ECF is considered, as indicated in Fig. 8. Thereafter, simulation for different cases of variations in the binding parameters (see Fig. 11, 14, 17 and 20) are considered to see how the distribution of drug within the brain is affected.

Initially, values for binding kinetics are fixed with $k_{1on} = 1 * 10^{-1}(\mu molL^{-1}s)^{-1}$, $k_{2on} = 1 * 10^{-2}(\mu molL^{-1}s)^{-1}$, $k_{1off} = 1 * 10^{-2}s^{-1}$ and $k_{2off} = 1 * 10^{-1}s^{-1}$ for Fig. 8. The drug compounds in the region of the brain ECF adjacent to the BBB distribute in huge amounts throughout the whole region next to the BBB for the first level of time $(t_1 = 2sec)$ (see Fig. 8(a)). At the second time level $(t_2 = 8sec)$ as indicated in Fig. 8(b), drug compounds distribute with a slight decrease in drug concentration within the brain ECF. Figure 8(b) shows that, drug concentration within the brain ECF decreases over almost the whole region of the brain ECF except a very few areas where the concentration is a bit higher. However, when the time further increases in Fig. 8(c), a significant decrease in amount of the drug concentration within the brain ECF is noticed. Thus, the drug concentration in Fig. 8(b) is less compared to Fig. 8(a) but reasonably higher compared to the concentration when time increases further to $t_3 = 14sec$ as indicated in Fig. 8(c).

In this case, the association rate in specific binding is the same as the dissociation rate in non-specific binding sites. Nevertheless, the association rate in non-specific binding is the same as the dissociation rate in specific binding. The association rate at specific binding sites is larger compared to that at non-specific sites, hence the drug compounds associates fast with the specific sites as compared to the non-specific sites. Moreover, the dissociation rate at non-specific binding sites is larger compared to the one at specific binding sites. This results into high dissociation of the drug at non-specific binding sites. Therefore, the drug distributes in non-specific binding sites with slightly large amount of concentration than in specific binding targets,

(see Fig. 9 and Fig.10). The plots (a), (b) and (c) in Fig. 8 indicate the distribution of drug in the brain ECF (ρ) for $t = 2s$, $t = 8s$ and $t = 14s$ respectively. Also, plots (a), (b) and (c) in Fig. 9 and Fig.10 indicate the distribution of drug in both specific (B_1) and non-specific binding sites (B_2) for $t = 2s$, $t = 8s$ and $t = 14s$ respectively.

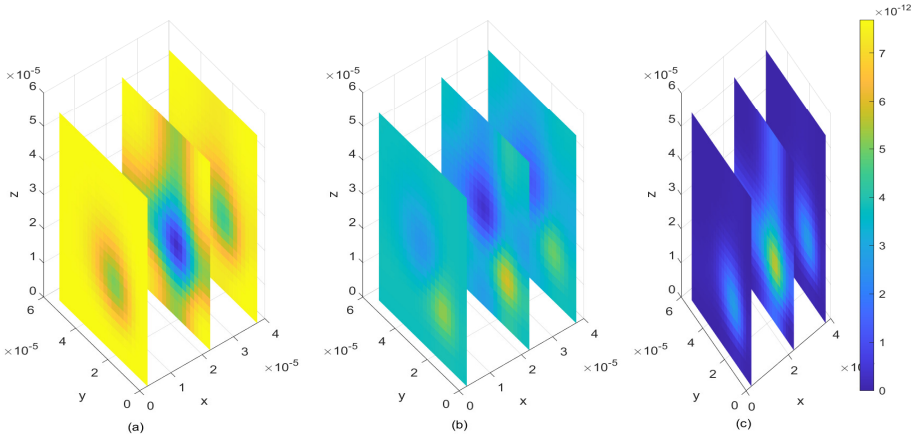

Figure 8: Drug distribution in brain ECF (ρ) for $k_{1on} = 1 * 10^{-1}(\mu molL^{-1}s)^{-1}$, $k_{2on} = 1 * 10^{-2}(\mu molL^{-1}s)^{-1}$, $k_{1off} = 1 * 10^{-2}s^{-1}$, and $k_{2off} = 1 * 10^{-1}s^{-1}$

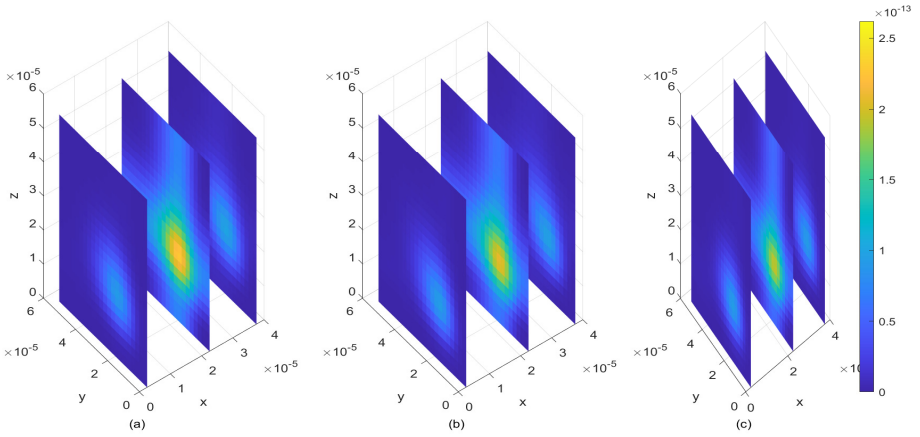

Figure 9: Drug distribution in specific binding sites (B_1) for $k_{1on} = 1 * 10^{-1}(\mu molL^{-1}s)^{-1}$, $k_{2on} = 1 * 10^{-2}(\mu molL^{-1}s)^{-1}$, $k_{1off} = 1 * 10^{-2}s^{-1}$, and $k_{2off} = 1 * 10^{-1}s^{-1}$

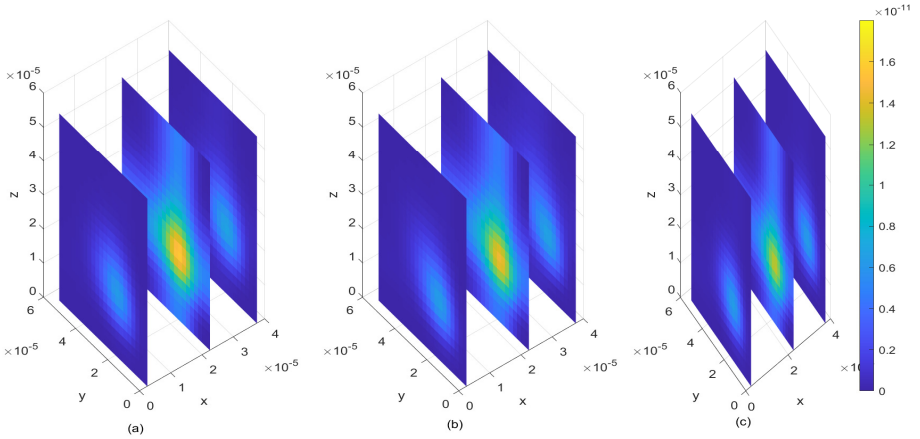

Figure 10: Drug distribution in non-specific binding sites (B_2) for $k_{1on} = 1 * 10^{-1}(\mu molL^{-1}s)^{-1}$, $k_{2on} = 1 * 10^{-2}(\mu molL^{-1}s)^{-1}$, $k_{1off} = 1 * 10^{-2}s^{-1}$, and $k_{2off} = 1 * 10^{-1}s^{-1}$

(i) Impact of varying dissociation rates $(k_{1,2off})$ while maintaining association rates $(k_{1,2on})$

The effect of drug binding kinetics, (k_{ion} and $k_{iof f}$,for $i = 1, 2$), on drug distribution within the brain with variations in dissociation rates is further assessed. In this particular case the association rate of specific binding sites $(k_{1on} = 1 * 10^{-1}(\mu molL^{-1}s)^{-1})$ is larger than the association rate at non-specific binding sites $(k_{2on} = 1 * 10^{-2}(\mu molL^{-1}s)^{-1})$. Also, the dissociation rate at non-specific binding sites $(k_{2off} = 3 * 10^{-0.2}s^{-1})$ is larger than the dissociation rate at specific binding sites $(k_{1off} = 5 * 10^{-1}s^{-1})$.

Initially at $(t_1 = 2sec)$, the concentration of drug in the brain ECF region next to the BBB is found to be considerably large and spread widely over that region (see Fig. 11(a)). Nevertheless, drug compounds within the brain ECF continue to spread with a slight decrease in concentration as time increases to $(t_2 = 8sec)$ (see Fig. 11(b)). Moreover, the concentration of drug tends to diminish to a lesser amount as time increases further to $(t_3 = 14sec)$, as shown in Fig. 11(c). Thus, in Fig. 11(a) and (b), the concentration of drug within the brain ECF at the first two-time levels exhibits a gradual decrease over the whole region of the brain ECF. Additionally, as the time further increases in Fig. 11(c), the drug concentration within the brain ECF becomes much more lesser due to absorption within the brain ECF. However, the drug concentration amount in the brain ECF for both Fig. 8 and 11 are almost the same.

Contrary to when small values of dissociation rates are considered in Fig. 8, the drug compounds

in Fig. 11 distribute more widely over the brain ECF region due to higher dissociation of drug compounds. Furthermore, the drug concentration in non-specific binding sites (see Fig. 13) is slightly more compared to the concentration in the specific binding targets (see Fig. 12). The plots (a), (b) and (c) in Fig. 11 indicate the distribution of drug in the brain ECF (ρ) for $t = 2s$, $t = 8s$ and $t = 14s$ respectively. Also, plots (a), (b) and (c) in Fig. 12 and Fig. 13 indicate the distribution of drug in both specific (B_1) and non-specific binding sites (B_2) for $t = 2s$, $t = 8s$ and $t = 14s$ respectively.

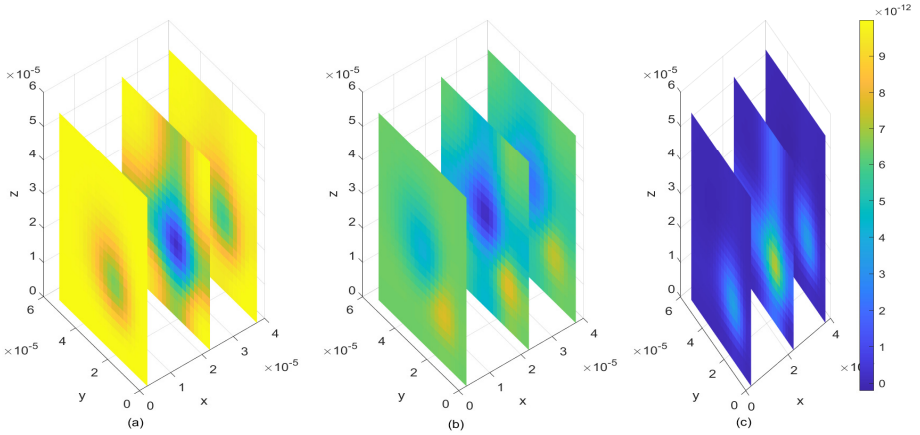

Figure 11: Drug distribution in brain ECF (ρ) for $k_{1on} = 1 * 10^{-1}(\mu molL^{-1}s)^{-1}$, $k_{2on} = 1 * 10^{-2}(\mu molL^{-1}s)^{-1}$, $k_{1off} = 5 * 10^{-1}s^{-1}$, and $k_{2off} = 3 * 10^{-0.2}s^{-1}$

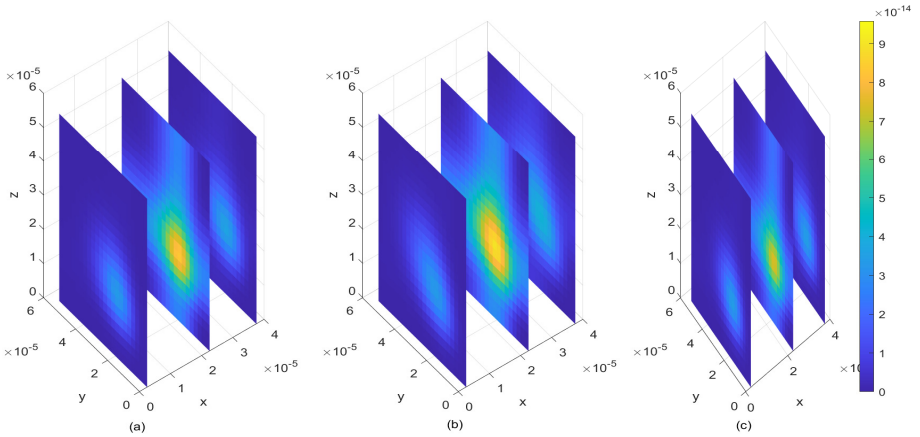

Figure 12: Drug distribution in specific binding sites (B_1) for $k_{1on} = 1 * 10^{-1}(\mu molL^{-1}s)^{-1}$, $k_{2on} = 1 * 10^{-2}(\mu molL^{-1}s)^{-1}$, $k_{1off} = 5 * 10^{-1}s^{-1}$, and $k_{2off} = 3 * 10^{-0.2}s^{-1}$

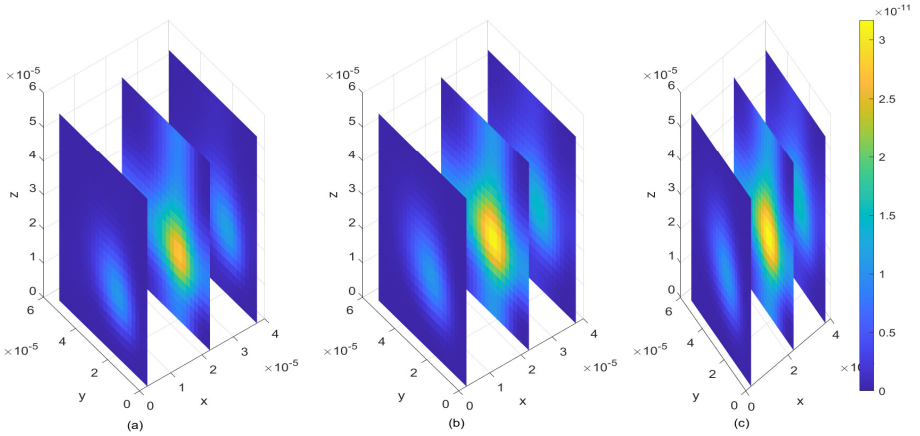

Figure 13: Drug distribution in non-specific binding sites (B_2) for $k_{1on} = 1 * 10^{-1}(\mu molL^{-1}s)^{-1}$, $k_{2on} = 1 * 10^{-2}(\mu molL^{-1}s)^{-1}$, $k_{1off} = 5 * 10^{-1}s^{-1}$, and $k_{2off} = 3 * 10^{-0.2}s^{-1}$

(ii) Impact of varying association rates $(k_{1,2on})$ while maintaining dissociation rates $(k_{1,2off})$

The effect of binding kinetics is also observed when the drug association rates are varied. With varied association rates, the drug compounds within the brain ECF doesn't spread widely even though the concentration within the brain ECF is considerably high compared to that in the binding sites, both specific and non-specific. Moreover, drug concentration in the non-specific binding sites is significantly large compared to that found in the specific binding sites.

The effect of change in association rates while maintaining the drug dissociation rates is assessed. The association rate in specific binding sites $(k_{1on} = 1 * 10^{-2}(\mu molL^{-1}s)^{-1})$ is greater than the one at non-specific binding sites $(k_{2on} = 1 * 10^{-3}(\mu molL^{-1}s)^{-1})$. In addition, the dissociation rate at the specific binding sites $(k_{1off} = 1 * 10^{-2}s^{-1})$ is less than the one at non-specific binding sites $(k_{1off} = 1 * 10^{-1}s^{-1})$. Simulation results show an increased concentration amount in non-specific binding sites (see Fig. 16) compared to the specific binding sites (see Fig. 15). Nevertheless, the distribution of drug concentration in the brain ECF slightly change with time in considerably small amount.

In addition, spatial variations of the location of drug concentration peak is observed in Fig. 14. Initially at $t_1 = 2sec$, the drug concentration peak within the brain ECF is observed in a region near W_{in} as indicated in Fig. 14(a). Moreover, the concentration peak in Fig. 14(a) covers a small area unlike in Fig. 14(b) and (c). When the time increases to $t_2 = 8sec$, the concentration

peak also spreads a little bit more as shown in Fig. 14(b). Moreover, when the time is further increased to $t_3 = 14sec$, the concentration peak within the brain ECF spread more over the region of the brain ECF in the direction of W_{out} as indicated in Fig. 14(c). Thus, the concentration peaks of drug within the brain ECF are found to cover different locations over the region when the association rates are altered. In addition, the drug compounds distribute within the brain ECF with an increasing pattern as time also increases. The plots (a), (b) and (c) in Fig. 14 indicate the distribution of drug in the brain ECF (ρ) for $t = 2s$, $t = 8s$ and $t = 14s$ respectively. Also, plots (a), (b) and (c) in Fig. 15 and Fig. 16 indicate the distribution of drug in both specific (B_1) and non-specific binding sites (B_2) for $t = 2s$, $t = 8s$ and $t = 14s$ respectively.

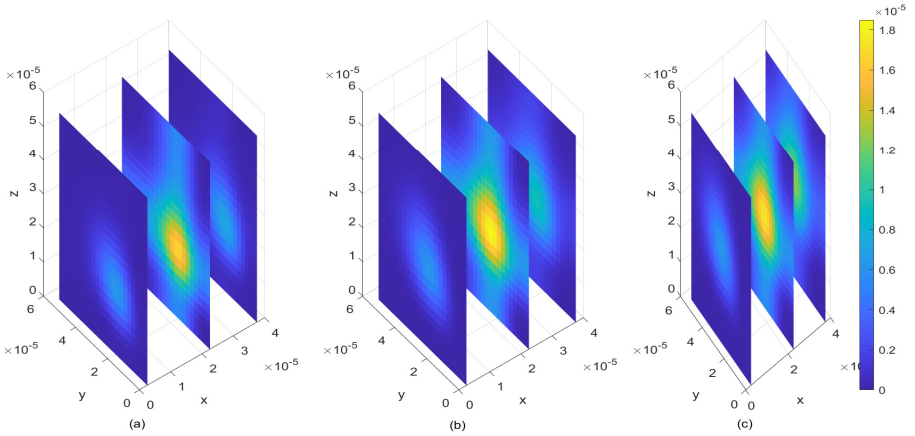

Figure 14: Drug distribution in the brain ECF (ρ) for $k_{1on} = 1 * 10^{-2}(\mu molL^{-1}s)^{-1}$, $k_{2on} = 1 * 10^{-3}(\mu molL^{-1}s)^{-1}$, $k_{1off} = 1 * 10^{-2}s^{-1}$, and $k_{2off} = 1 * 10^{-1}s^{-1}$

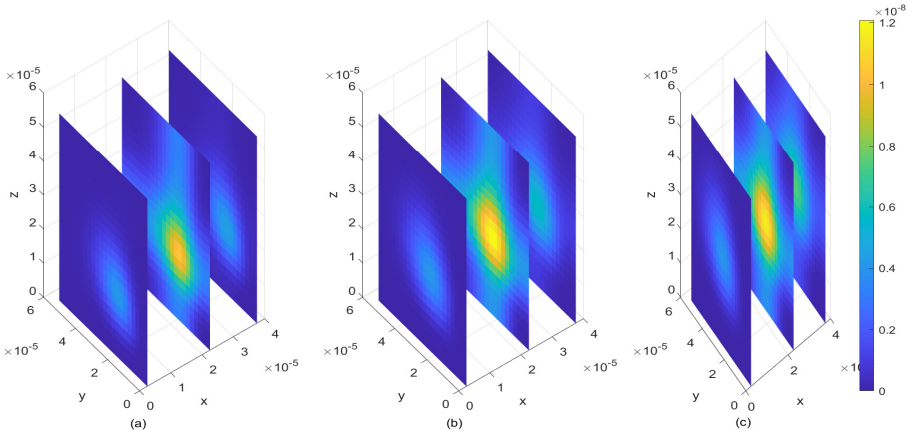

Figure 15: Drug distribution in specific binding sites (B_1) for $k_{1on} = 1 * 10^{-2}(\mu molL^{-1}s)^{-1}$, $k_{2on} = 1 * 10^{-3}(\mu molL^{-1}s)^{-1}$, $k_{1off} = 1 * 10^{-2}s^{-1}$, and $k_{2off} = 1 * 10^{-1}s^{-1}$

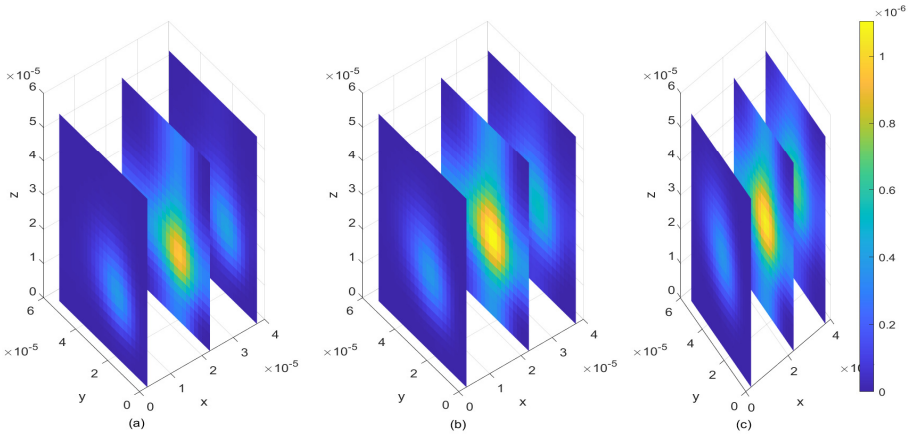

Figure 16: Drug distribution in non-specific binding sites (B_2) for $k_{1on} = 1 * 10^{-2}(\mu molL^{-1}s)^{-1}$, $k_{2on} = 1 * 10^{-3}(\mu molL^{-1}s)^{-1}$, $k_{1off} = 1 * 10^{-2}s^{-1}$, and $k_{2off} = 1 * 10^{-1}s^{-1}$

(iii) Impact of varying both association and dissociation rates, $(k_{1,2on})$ and $(k_{1,2off})$ simultaneously

Furthermore, simultaneous variations in both association and dissociation rates effect on the distribution of drug within the brain ECF is assessed. In Fig. 17, firstly the alteration in both association rate and dissociation rates for specific binding sites ($k_{1on} = 0.5(\mu molL^{-1}s)^{-1}$ and $k_{1off} = 2 * 10^{-1}s^{-1}$ respectively) is done while the association and dissociation rates for non-specific remain unchanged ($k_{2on} = 1 * 10^{-2}(\mu molL^{-1}s)^{-1}$ and $k_{2off} = 1 * 10^{-1}s^{-1}$

respectively). Thereafter, the association and dissociation rates for non-specific binding sites are varied with values ($k_{2on} = 2.5 * 10^{-4}(\mu molL^{-1}s)^{-1}$ and $k_{2off} = 1.5 * 10^{-3}s^{-1}$ respectively) while maintaining those for specific binding sites i.e. ($k_{1on} = 1(\mu molL^{-1}s)^{-1}$ and $k_{1off} = 1 * 10^{-2}s^{-1}$ respectively), for Fig. 20. Simulation results for Fig. 17 show that drug distributes widely within the region of the brain ECF for the first two-time levels ($t_1 = 2sec$ and $t_2 = 8sec$) with significantly small concentration as indicated by Fig. 17(a) and (b). However, there is a gradual change in the coverage of drug compounds in Fig. 17(a) and (b) whereby the drug compounds decrease significantly in relation to an increase in time. Nonetheless, the results in Fig. 17(c) show a higher decrease in amount of drug compounds within the brain ECF when the time increases further to $t_3 = 14sec$.

Contrarily, the results in Fig. 20 show that, the drug distributes over the brain ECF region with spatial variations in the location of the concentration peaks. The spatial variations of the location of drug concentration peak in Fig. 20 is initially observed at $t_1 = 2sec$. The drug concentration peak within the brain ECF at $t_1 = 2sec$ is observed in a region near W_{in} as indicated in Fig. 20(a). Moreover, the concentration peak in Fig. 20(a) covers a small area unlike in Fig. 20(b) and (c). When the time increases to $t_2 = 8sec$, the concentration peak also spreads a little wider as shown in Fig. 20(b). Additionally, when the time increases further to $t_3 = 14sec$, the concentration peak within the brain ECF spread more over the region of the brain ECF in the direction of W_{out} as indicated in Fig. 20(c). Thus, the concentration peaks of drug within the brain ECF are found to cover different locations over the region when the association rates are altered. Moreover, the drug compounds distribute within the brain ECF with an increasing pattern as time also increases. However, the concentration of drug in Fig. 20 is generally higher than the concentration in Fig. 17.

When the parameters for specific binding are varied, the amount of drug concentration in specific binding sites (see Fig. 18) is smaller than the concentration in non-specific binding sites (see Fig. 19). In addition, when parameters for non-specific binding are also varied, the concentration of drug in both specific and non-specific binding sites is almost the same as indicated by Fig. 21 and Fig. 22 respectively. The plots (a), (b) and (c) in Fig. 17 and Fig. 20 indicate the distribution of drug in the brain ECF (ρ) for $t = 2s$, $t = 8s$ and $t = 14s$ respectively. Also, plots (a), (b) and (c) in Fig. 18, 19, 21 and 22 indicate the distribution of drug in both specific (B_1) and non-specific binding sites (B_2) for $t = 2s$, $t = 8s$ and $t = 14s$ respectively.

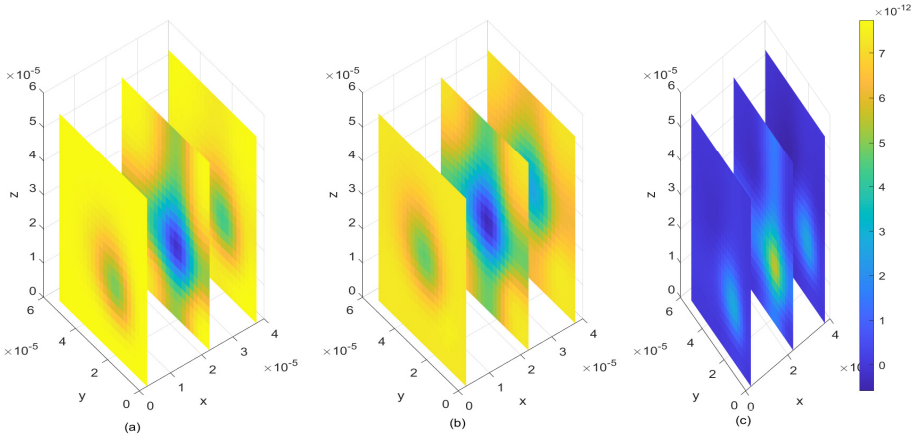

Figure 17: Drug distribution in the brain ECF (ρ) for $k_{1on} = 0.5(\mu molL^{-1}s)^{-1}$, $k_{2on} = 1 * 10^{-2}(\mu molL^{-1}s)^{-1}$, $k_{1off} = 2 * 10^{-1}s^{-1}$, and $k_{2off} = 1 * 10^{-1}s^{-1}$

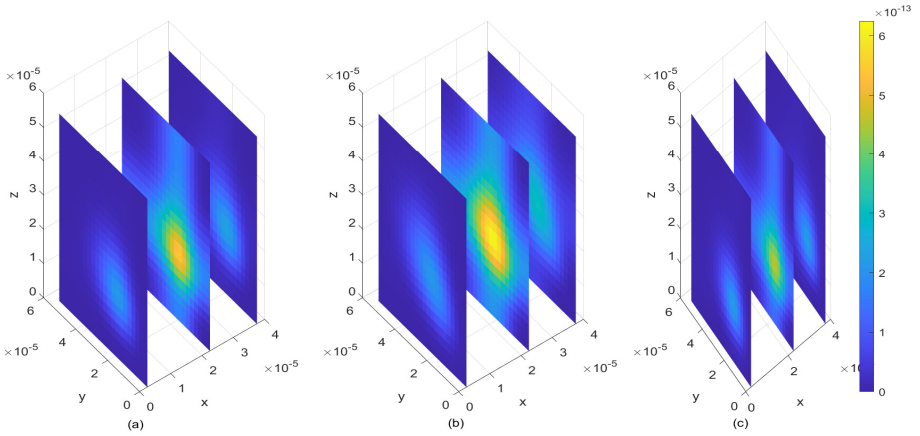

Figure 18: Drug distribution in specific binding sites (B_1) for $k_{1on} = 0.5(\mu molL^{-1}s)^{-1}$, $k_{2on} = 1 * 10^{-2}(\mu molL^{-1}s)^{-1}$, $k_{1off} = 2 * 10^{-1}s^{-1}$, and $k_{2off} = 1 * 10^{-1}s^{-1}$

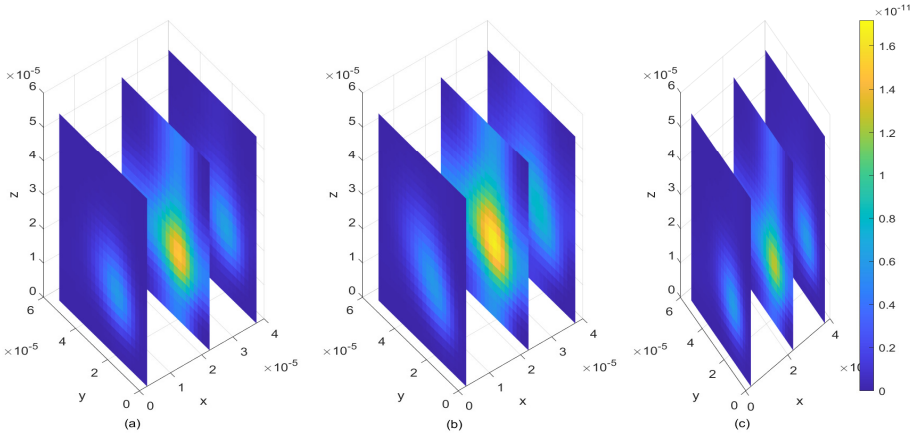

Figure 19: Drug distribution in non-specific binding sites (B_2) for $k_{1on} = 0.5(\mu molL^{-1}s)^{-1}$, $k_{2on} = 1 * 10^{-2}(\mu molL^{-1}s)^{-1}$, $k_{1off} = 2 * 10^{-1}s^{-1}$, and $k_{2off} = 1 * 10^{-1}s^{-1}$

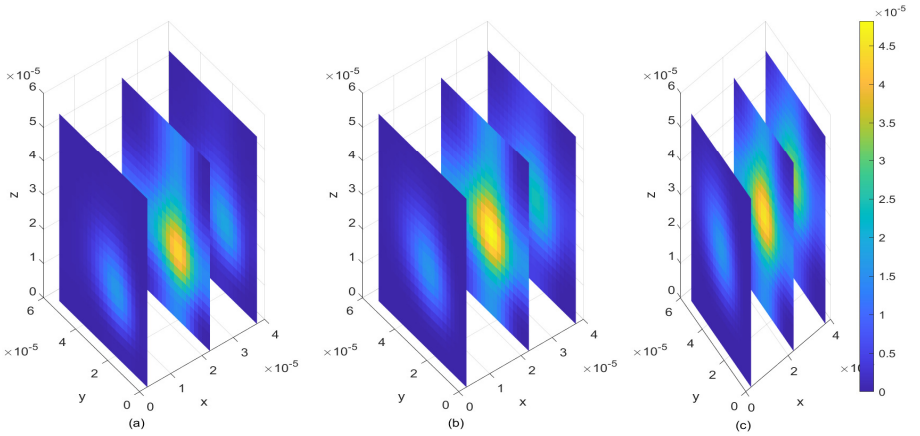

Figure 20: Drug distribution in the brain ECF (ρ) for $k_{1on} = 1 * 10^{-1}(\mu molL^{-1}s)^{-1}$, $k_{2on} = 2.5 * 10^{-4}(\mu molL^{-1}s)^{-1}$, $k_{1off} = 1 * 10^{-2}s^{-1}$, and $k_{2off} = 1.5 * 10^{-3}s^{-1}$

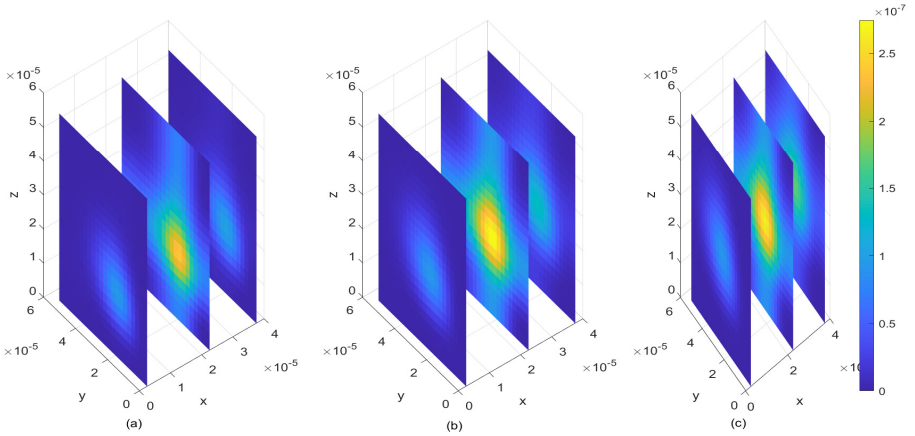

Figure 21: Drug distribution in specific binding sites (B_1) for $k_{1on} = 1 * 10^{-1}(\mu molL^{-1}s)^{-1}$, $k_{2on} = 2.5 * 10^{-4}(\mu molL^{-1}s)^{-1}$, $k_{1off} = 1 * 10^{-2}s^{-1}$, and $k_{2off} = 1.5 * 10^{-3}s^{-1}$

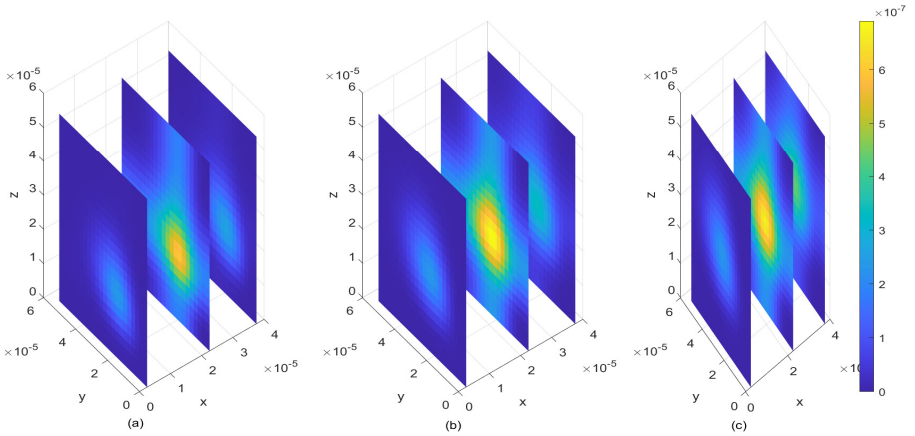

Figure 22: Drug distribution in non-specific binding sites (B_2) for $k_{1on} = 1 * 10^{-1}(\mu molL^{-1}s)^{-1}$, $k_{2on} = 12.5 * 10^{-4}(\mu molL^{-1}s)^{-1}$, $k_{1off} = 1 * 10^{-2}s^{-1}$, and $k_{2off} = 1.5 * 10^{-3}s^{-1}$

4.2 Discussion

In the current study, a mathematical model is formulated and simulated through which the effect of binding kinetics in drug distribution within the brain is determined. The model formulated in the current study is an augmentation of the model earlier developed by Vendel *et al.* (2020). In this study, the bidirectional bulk flow of the brain ECF was considered contrary to the model developed by Vendel *et al.* (2020) which considers only one direction of the bulk flow of the brain ECF. In addition, the distinction is made between specific and non-specific binding sites

along with the subsequent drug distribution in respective binding sites through simulated plots.

The model Equations are discretised through the implicit FDM. The discretised Equations are then used for simulation from which different plots describing drug distribution along blood plasma and brain ECF domains are obtained. First, the drug distribution within blood plasma is discussed. Then, different cases of association and dissociation rates in specific and non-specific binding sites (k_{ion} and $k_{iof f}$ respectively, for $(i = 1, 2)$) are considered to determine the impacts they impose on drug distribution within the brain ECF.

The findings of this study show how blood flow rate and BBB permeability influence both drug concentration within blood plasma and the distribution of drug compounds in that domain. The simultaneous increase of the BBB permeability and blood flow rate affect the short term distribution of drug compounds in the blood plasma, yet with a high BBB permeability there is an even distribution of drug within the brain. Nevertheless, drug compounds in the brain ECF are influenced by both the permeability of BBB and blood flow rate. However, the concentrations at the binding sites contribute to variations in distribution of drug compounds in the brain ECF.

Contrary to the study by Vendel *et al.* (2020), the current study investigates the effect of drug-binding kinetics in drug distribution in the brain with variations in binding parameter values. Different cases of varied binding parameter values are considered. The results show that, when the higher values for dissociation rates are used while maintaining those for association rates, the gradual decrease in drug concentration within the brain ECF is observed. Also, the drug concentration within the brain ECF becomes much lesser due to drug absorption within the brain ECF. When the alteration of association rates with the unchanged dissociation rates is considered, the concentration peaks of drug within the brain ECF are found to cover different locations within the brain ECF. Moreover, the drug compounds within the brain ECF distribute with an increasing pattern. The results of simultaneous variations in both association and dissociation rates for specific binding sites show that, the drug concentration within the brain ECF decrease significantly in relation to an increase in time. Nevertheless, the results of simultaneous variations in both association and dissociation rates for non-specific binding sites show that, the drug distributes in the brain ECF region with the subsequent spatial variations in locations of concentration peaks from the region near W_{in} towards the direction of W_{out} region.

CHAPTER FIVE

CONCLUSION AND RECOMMENDATIONS

5.1 Conclusion

The 3- dimensional model developed in this study aimed to determine the effect of drug binding kinetics in spatial drug distribution within the brain. The model integrates the key components involved in drug distribution within the brain, such are; drug transport across the BBB, drug distribution within the brain ECF and drug binding kinetics. In addition, the model incorporates the bidirectional bulk flow of the brain ECF to enhance the visualization of drug distribution within the brain and explore how the binding kinetics affect the whole process of drug distribution.

The results of this study showed an enhanced visualization of drug distribution within both blood plasma and brain ECF domains. Additionally, the research findings showed that the transport across the BBB and blood flow rate affect drug distribution in both blood plasma and brain ECF. Effects of binding kinetics in drug distribution were also observed through varied binding parameters where different cases of variations were considered. The findings showed a substantial decrease of drug concentration in the brain ECF when higher values for dissociation rates were considered while maintaining those for association rates. Contrarily, the drug distribution within the brain ECF were observed with an increasing trend when the association rates were altered. In another case, it was found that the drug concentration within the brain ECF decreases significantly as time rises when both association and dissociation rates for specific binding sites are varied simultaneously. Nevertheless, when both association and dissociation rates for non-specific binding sites are varied, the results of simultaneous variations indicated that the drug distributes in the brain ECF region with spatial differences in concentration peaks across the brain ECF region.

5.2 Recommendations

Understanding how the drug is distributed within human brain is still very challenging. This challenge poses an obstruction towards potential therapeutic measures for brain associated diseases or infections. Therefore, 3-dimensional models are recommended as powerful tools that can be used to study the inter-dependencies of complex factors involved in drug distribution within the brain. Additionally, the developed 3-dimensional model provided very insightful and

useful information about drug distribution within the brain, however much need to be unveiled especially on the factors that were not considered in the model developed in this study, such are; drug metabolism, perfusion rate, lipid solubility and degree of ionization of the drug. Therefore, this study recommends the integration of the aforementioned factors for there to be more fine-tuned results and better visualization of the impact of each or combination of the factors in drug distribution within the brain.

REFERENCES

Ball, K., Bouzom, F., Scherrmann, J. M., Walther, B., & Declèves, X. (2014). A physiologically based modeling strategy during preclinical CNS drug development. *Molecular Pharmaceutics*, *11*(3), 836–848.

Barar, J., Rafi, M. A., Pourseif, M. M., & Omidi, Y. (2016). Blood-brain barrier transport machineries and targeted therapy of brain diseases. *BioImpacts: BI*, *6*(4), 225-248.

Bickel, U. (2005). How to measure drug transport across the blood-brain barrier. *NeuroRx*, *2*(1), 15–26.

Clarelli, F., Liang, J., Martinecz, A., Heiland, I., & Zur-Wiesch, P. A. (2020). Multi-scale modeling of drug binding kinetics to predict drug efficacy. *Cellular and Molecular Life Sciences*, *77*(3), 381–394.

De-Witte, W. E. A., Vauquelin, G., Van-Der, G. P. H., & De-Lange, E. C. M. (2017). The influence of drug distribution and drug-target binding on target occupancy: The rate-limiting step approximation. *European Journal of Pharmaceutical Sciences*, *109*, S83-S89.

De-Witte, W. E. A., Danhof, M., Van-Der, G. P. H., & De-Lange, E. C. M. (2016). In vivo target residence time and kinetic selectivity: The association rate constant as determinant. *Trends in Pharmacological Sciences*, *37*(10), 831–842.

De-Witte, W. E. A., Rottschäfer, V., Danhof, M., Van-Der, G. P. H., Peletier, L. A., & De-Lange, E. C. M. (2018). Modelling the delay between pharmacokinetics and EEG effects of morphine in rats: binding kinetic versus effect compartment models. *Journal of Pharmacokinetics and Pharmacodynamics*, *45*(4), 621–635.

Einstein, A. (1905). *Investigations on the Theory of Brownian Movement. In R. Futh (Ed.) Dutton, New York.* https://www.maths.usyd.edu.au/u/UG/SM/MATH3075/r/Einstein_1905.pdf

Hawkins, B. T., & Davis, T. P. (2005). The blood-brain barrier/neurovascular unit in health and disease. *Pharmacological Reviews*, *57*(2), 173–185.

Hladky, S. B., & Barrand, M. A. (2016). Fluid and ion transfer across the blood-brain and blood-cerebrospinal fluid barriers: A comparative account of mechanisms and roles. *Fluids and Barriers of the CNS*, *13*(1), 1–69.

Karbowski, J. (2011). Scaling of brain metabolism and blood flow in relation to capillary and neural scaling. *PloS One*, *6*(10), 1-11.

Langhoff, W., Riggs, A., & Hinow, P. (2018). Scaling behavior of drug transport and absorption in in silico cerebral capillary networks. *PloS One*, *13*(7), 1-14.

Nhan, T., Burgess, A., Lilge, L., & Hynynen, K. (2014). Modeling localized delivery of Doxorubicin to the brain following focused ultrasound enhanced blood-brain barrier permeability. *Physics in Medicine & Biology*, *59*(20), 5987-6004.

Nicholson, C., Chen, K. C., Hrabětová, S., & Tao, L. (2000). Diffusion of molecules in brain extracellular space: theory and experiment. *Progress in Brain Research*, *125*, 129–154.

Owens, J. (2007). Determining druggability. *Nature Reviews Drug Discovery*, *6*(3), 71-75.

Pardridge, W. M. (2005). The blood-brain barrier: Bottleneck in brain drug development. *NeuroRx*, *2*(1), 3–14. https://doi.org/10.1602/neurorx.2.1.3

Pardridge, W. M. (2016). CSF, blood-brain barrier, and brain drug delivery. *Expert Opinion on Drug Delivery*, *13*(7), 963–975.

Paul, A. (2019). *Drug Distribution. In Introduction to Basics of Pharmacology and Toxicology.* https://link.springer.com/chapter/10.1007/978-981-32-9779-1_5

Reichel, A. (2015). *Pharmacokinetics of CNS penetration. Blood-Brain Barrier in Drug Discovery: Optimizing Brain Exposure of CNS Drugs and Minimizing Brain Side Effects for Peripheral Drugs*. https://www.ncbi.nlm.nih.gov/nlmcatalog/101643550

Schlageter, K. E., Molnar, P., Lapin, G. D., & Groothuis, D. R. (1999). Microvessel organization and structure in experimental brain tumors: Microvessel populations with distinctive structural and functional properties. *Microvascular Research*, *58*(3), 312–328.

Sim, D. S. M. (2015). *Drug distribution. In Pharmacological Basis of Acute Care.* https://www.springer.com/gp/book/9783319103853

Sweeney, M. D., Zhao, Z., Montagne, A., Nelson, A. R., & Zlokovic, B. V. (2019). Blood-brain barrier from physiology to disease and back. *Physiological Reviews*, *99*(1), 21–78.

Sykes, D. A., Stoddart, L. A., Kilpatrick, L. E., & Hill, S. J. (2019). Binding kinetics of ligands acting at GPCRs. *Molecular and Cellular Endocrinology*, *485*, 9–19.

Syková, E., & Nicholson, C. (2008). Diffusion in brain extracellular space. *Physiological Reviews*, *88*(4), 1277–1340.

Syvänen, S., Xie, R., Sahin, S., & Hammarlund-Udenaes, M. (2006). Pharmacokinetic consequences of active drug efflux at the blood--brain barrier. *Pharmaceutical Research*, *23*(4), 705–717.

Tasso, L., Bettoni, C. C., & Costa, T. D. (2008). Pharmacokinetic plasma profile and bioavailability evaluation of gatifloxacin in rats. *Latin American Journal of Pharmacy*, *27*(2), 270–273.

Tata, D. A., & Anderson, B. J. (2002). A new method for the investigation of capillary structure. *Journal of Neuroscience Methods*, *113*(2), 199–206.

Upadhyay, R. K. (2014). Drug delivery systems, CNS protection, and the blood brain barrier. *BioMed Research International*, *2014*, 1-37. https://doi.org/10.1155/2014/869269

Vendel, E., Rottschäfer, V., & De-Lange, E. C. (2020). A 3D brain unit model to further improve prediction of local drug distribution within the brain. *PloS One*, *15*(9), 1-24.

Vendel, E., Rottschäfer, V., & De-Lange, E. C. M. (2019a). Improving the prediction of local drug distribution profiles in the brain with a new 2D mathematical model. *Bulletin of Mathematical Biology*, *81*(9), 3477–3507.

Vendel, E., Rottschäfer, V., & De-Lange, E. C. M. (2019b). The need for mathematical modelling of spatial drug distribution within the brain. *Fluids and Barriers of the CNS*, *16*(1), 12-33.

Westerhout, J., Den-Berg, D. J., Hartman, R., Danhof, M., & De-Lange, E. C. M. (2014). Prediction of methotrexate CNS distribution in different species-Influence of disease conditions. *European Journal of Pharmaceutical Sciences*, *57*, 11–24.

Westerhout, J., Smeets, J., Danhof, M., & De-Lange, E. C. M. (2013). The impact of P-gp functionality on non-steady state relationships between CSF and brain extracellular fluid. *Journal of Pharmacokinetics and Pharmacodynamics*, *40*(3), 327–342.

Wong, A., Ye, M., Levy, A., Rothstein, J., Bergles, D., & Searson, P. C. (2013). The blood-brain barrier: An engineering perspective. *Frontiers in Neuroengineering*, *6*, 7-22.

Yamamoto, Y., Välitalo, P. A., Van-Den B. D. J., Hartman, R., Van-Den, B. W., Wong, Y. C., Huntjens, D. R., Proost, J. H., Vermeulen, A., Krauwinkel, W., Bakshi, S., Aranzana-Climent, V., Claire, S. M., Fizelier, D., Couet, W., Danhof, M., J., Van-Der, G. P. H., & De-Lange, E. C. M. (2017). A generic multi-compartmental CNS distribution model structure for 9 drugs allows prediction of human brain target site concentrations. *Pharmaceutical Research*, *34*(2), 333–351.

APPENDICES

APPENDIX I: Code for Simulations

```
function drug_Conc3()
clear all; clc; close all

%% Discretize our space
r=2.5*10^(-6);%radius of brain capillary
lcap=5*10^(-5);%inter-capillary distance
L=lcap+2*r; %Length of the cube
x=0:r:L; y=0:r:L; z=0:r:L; h=r;N=length(x);
%% Discretize our time
dt=1;t=0:dt:15;

%% define parameter values
F=1;Dose=0.5;
Ka=2*10^(-4);Ke=5*10^(-5);
Vd=0.2;
vblood=1*10^(-6); %%%volume of blood
Dstar=2.5*10^(-16); %%%effective diffusion coefficient
VECF=0.5*10^(-6); %%%brain ECF bulk flow velocity
P=0.1*10^(-7);Tin=0.1*10^(-12);Tout=0.1*10^(-12);
Kin=1*10^2;Kout=1*10^2;Sa=0.1*10^(-7);
B1tot=5*10^(-2);
k1on=1*10^(-1); %%%specific association constant
k1off=1*10^(-2); %%%specific dissociation constant
B2tot=5*10^(1);
k2on=2.5*10^(-4); %%%non-specific association constant
k2off=1.5*10^(-3); %%%non-specific dissociation constant

beta=(-vblood*dt)/(2*h);
alpha=(2500*Dstar*dt)/(h^2);gamma=(VECF*dt)/(2*h);omega1=k1on*
```

```
dt;omega2=k2on*dt;tau1=k1off*dt;tau2=k2off*dt;


%% setting up the conditions
f=zeros(length(x),length(y),length(z),length(t));
miu=zeros(length(x),length(y),length(z),length(t));
rho=zeros(length(x),length(y),length(z),length(t));
B1=zeros(length(x),length(y),length(z),length(t));
B2=zeros(length(x),length(y),length(z),length(t));

%=========================================================
%%Initial Conditions
miu(:,:,:,1)=0; %the Initial Condition (9)
rho(:,:,:,1)=0; %the Initial Condition (9)
B1(:,:,:,1)=0; %the Initial Condition (9)
B2(:,:,:,1)=0; %the Initial Condition (9)
%=========================================================
for n=1:length(t)
miu(1:2,1:2,1:2,n)=((F*Dose*Ka)/(Vd*(Ka-Ke)))*(exp(-Ke*t(n))-
    exp(-Ka*t(n))); %%%miu-belongs-Win Boundary Condition (15)
f(1:2,1:2,1:2,n)=fminrho(miu(1:2,1:2,1:2,n),rho(1:2,1:2,1:2,n))
    ;
rho(1:2,1:2,1:2,n)=rho(1:2,1:2,1:2,n)+(h/Dstar)*f(1:2,1:2,1:2,n
    );
end
%=========================================================

%%% (implicit) Finite Difference Method
for n=1:length(t)-1
 for i=2:length(x)-1
      for j=2:length(y)-1
          for k=2:length(z)-1
```

```
        miu(1,1:length(y),1:length(z),n)=miu(2,1:length(y)
            ,1:length(z),n); %%%x=0 Boundary Condition (12)
        miu(N,1:length(y),1:length(z),n)=miu(N-1,1:length(y
            ),1:length(z),n); %%%x=xr Boundary Condition
            (12)
        miu(1:length(x),1,1:length(z),n)=miu(1:length(x)
            ,2,1:length(z),n); %%%y=0 Boundary Condition
            (12)
        miu(1:length(x),N,1:length(z),n)=miu(1:length(x),N
            -1,1:length(z),n); %%%y=yr Boundary Condition
            (12)
        miu(1:length(x),1:length(y),1,n)=miu(1:length(x),1:
            length(y),2,n); %%%z=0 Boundary Condition (12)
        miu(1:length(x),1:length(y),N,n)=miu(1:length(x),1:
            length(y),N-1,n); %%%z=zr Boundary Condition
            (12)

%
    %=================================================================


        rho(1,j,k,n)=rho(2,j,k,n); %%%Wsub(ECF)&&del(W) in
            x-direction at 1st boundary (14)
        rho(N,j,k,n)=rho(N-1,j,k,n); %%%Wsub(ECF)&&del(W)
            in x-direction at 2nd boundary (14)
        rho(i,j,1,n)=rho(i,j,2,n); %%%Wsub(ECF)&&del(W) in
            z-direction at 1st boundary (14)
        rho(i,j,N,n)=rho(i,j,N-1,n); %%%Wsub(ECF)&&del(W)
            in z-direction at 2nd boundary (14)

    f(i,j,k,n)=fminrho(miu(i,j,k,n),rho(i,j,k,n));
    miu(i,j,k,n+1)=miu(i,j,k,n)+beta*(miu(i+1,j,k,n)-miu(i-1,j
```

```
        ,k,n+1)) ...
              +beta*(miu(i,j+1,k,n)-miu(i,j-1,k,n+1))+beta*(miu(
                  i,j,k+1,n)-miu(i,j,k-1,n+1));
    %
        ==========================================================

    rho(i,j,k,n+1)=(1-6*alpha)*rho(i,j,k,n) ...
        +alpha*(rho(i+1,j,k,n)+rho(i-1,j,k,n+1)+rho(i,j+1,k,n)+
            rho(i,j-1,k,n+1)+rho(i,j,k+1,n)+rho(i,j,k-1,n+1)) ...
        -gamma*(rho(i+1,j,k,n)-rho(i-1,j,k,n+1)+rho(i,j+1,k,n)-
            rho(i,j-1,k,n+1)+rho(i,j,k+1,n)-rho(i,j,k-1,n+1)) ...
        -omega1*(rho(i,j,k,n))*(B1tot-B1(i,j,k,n))+tau1*B1(i,j,
            k,n) ...
        -omega2*(rho(i,j,k,n))*(B2tot-B2(i,j,k,n))+tau2*B1(i,j,
            k,n); %%%diffusion of drug in the brain ECF  (6)
    %
        ==========================================================

    B1(i,j,k,n+1)=(1-tau1)*B1(i,j,k,n)+omega1*rho(i,j,k,n)*(
        B1tot-B1(i,j,k,n)); %%%specific binding  (7)
    %
        ==========================================================

    B2(i,j,k,n+1)=(1-tau2)*B2(i,j,k,n)+omega2*rho(i,j,k,n)*(
        B2tot-B2(i,j,k,n)); %%%non-specific binding (8)

      end
    end
  end
end

time1=find(t==2);time2=find(t==8);time3=find(t==14);
```

```
figure('DefaultAxesFontSize',12)
subplot(1,3,1)
VB1=zeros(length(x),length(y),length(z));
for i=1:length(x)
    VB1_yz(i,:,:)=B1(N-1,:,:,time1);
    for j=1:length(y)
        VB1_xz(:,j,:)=B1(:,N-1,:,time1);
        for k=1:length(z)
            VB1_xy(:,:,k)=B1(:,:,N-1,time1);
            VB1(i,j,k)=VB1_xy(i,j,k)+VB1_yz(i,j,k)+VB1_xz(i,j,k
                );
        end
    end
end
xslice=[x(2),x(10),x(16)]; yslice=[]; zslice=[];
slice(x,y,z,VB1,xslice,yslice,zslice); xlabel('x'); ylabel('y');
   zlabel('z');
shading flat

subplot(1,3,2)
VB1=zeros(length(x),length(y),length(z));
for i=1:length(x)
    VB1_yz(i,:,:)=B1(N-1,:,:,time2);
    for j=1:length(y)
        VB1_xz(:,j,:)=B1(:,N-1,:,time2);
        for k=1:length(z)
            VB1_xy(:,:,k)=B1(:,:,N-1,time2);
            VB1(i,j,k)=VB1_xy(i,j,k)+VB1_yz(i,j,k)+VB1_xz(i,j,k
                );
        end
    end
end
```

```
xslice=[x(2),x(10),x(16)]; yslice=[]; zslice=[];
slice(x,y,z,VB1,xslice,yslice,zslice); xlabel('x'); ylabel('y');
   zlabel('z');
shading flat

subplot(1,3,3)
VB1=zeros(length(x),length(y),length(z));
for i=1:length(x)
    VB1_yz(i,:,:)=B1(N-1,:,:,time3);
    for j=1:length(y)
        VB1_xz(:,j,:)=B1(:,N-1,:,time3);
        for k=1:length(z)
            VB1_xy(:,:,k)=B1(:,:,N-1,time3);
            VB1(i,j,k)=VB1_xy(i,j,k)+VB1_yz(i,j,k)+VB1_xz(i,j,k
                );
        end
    end
end
xslice=[x(2),x(10),x(16)]; yslice=[]; zslice=[];
slice(x,y,z,VB1,xslice,yslice,zslice); xlabel('x'); ylabel('y');
   zlabel('z');
shading flat
colorbar('eastoutside')


time1=find(t==2); time2=find(t==8); time3=find(t==14);
figure('DefaultAxesFontSize',12)
subplot(1,3,1)
VB2=zeros(length(x),length(y),length(z));
for i=1:length(x)
    VB2_yz(i,:,:)=B2(N-1,:,:,time1);
    for j=1:length(y)
```

```
        VB2_xz(:,j,:)=B2(:,N-1,:,time1);
        for k=1:length(z)
            VB2_xy(:,:,k)=B2(:,:,N-1,time1);
            VB2(i,j,k)=VB2_xy(i,j,k)+VB2_yz(i,j,k)+VB2_xz(i,j,k
                );
        end
    end
end
xslice=[x(2),x(10),x(16)]; yslice=[]; zslice=[];
slice(x,y,z,VB2,xslice,yslice,zslice); xlabel('x'); ylabel('y');
   zlabel('z');
shading flat

subplot(1,3,2)
VB2=zeros(length(x),length(y),length(z));
for i=1:length(x)
    VB2_yz(i,:,:)=B2(N-1,:,:,time2);
    for j=1:length(y)
        VB2_xz(:,j,:)=B2(:,N-1,:,time2);
        for k=1:length(z)
            VB2_xy(:,:,k)=B2(:,:,N-1,time2);
            VB2(i,j,k)=VB2_xy(i,j,k)+VB2_yz(i,j,k)+VB2_xz(i,j,k
                );
        end
    end
end
xslice=[x(2),x(10),x(16)]; yslice=[]; zslice=[];
slice(x,y,z,VB2,xslice,yslice,zslice); xlabel('x'); ylabel('y');
   zlabel('z');
shading flat

subplot(1,3,3)
```

```
VB2=zeros(length(x),length(y),length(z));
for i=1:length(x)
    VB2_yz(i,:,:)=B2(N-1,:,:,time3);
    for j=1:length(y)
        VB2_xz(:,j,:)=B2(:,N-1,:,time3);
        for k=1:length(z)
            VB2_xy(:,:,k)=B2(:,:,N-1,time3);
            VB2(i,j,k)=VB2_xy(i,j,k)+VB2_yz(i,j,k)+VB2_xz(i,j,k
                );
        end
    end
end
xslice=[x(2),x(10),x(16)]; yslice=[]; zslice=[];
slice(x,y,z,VB2,xslice,yslice,zslice); xlabel('x'); ylabel('y');
   zlabel('z');
shading flat
colorbar('eastoutside')

%explore better visualization of the 3D functions
time1=find(t==2); time2=find(t==8); time3=find(t==14);
figure('DefaultAxesFontSize',12)
subplot(1,3,1)
Vmiu = zeros(length(x),length(y),length(z));
for i=1:length(x)
    Vmiu_yz(i,:,:)=miu(N-1,:,:,time1);
   for j=1:length(y)
        Vmiu_xz(:,j,:)=miu(:,N-1,:,time1);
        for k=1:length(z)
            Vmiu_xy(:,:,k)=miu(:,:,N-1,time1);
            Vmiu(i,j,k)=Vmiu_xy(i,j,k)+Vmiu_yz(i,j,k)+Vmiu_xz(i,
                j,k);
        end
```

```
    end
end
xslice = [x(2),x(10),x(16)]; yslice = []; zslice = [];
slice(x,y,z,Vmiu,xslice,yslice,zslice); xlabel('x'); ylabel('y');
    zlabel('z')
shading flat

subplot(1,3,2)
Vmiu = zeros(length(x),length(y),length(z));
for i=1:length(x)
     Vmiu_yz(i,:,:)=miu(N-1,:,:,time2);
    for j=1:length(y)
        Vmiu_xz(:,j,:)=miu(:,N-1,:,time2);
        for k=1:length(z)
            Vmiu_xy(:,:,k)=miu(:,:,N-1,time2);
            Vmiu(i,j,k)=Vmiu_xy(i,j,k)+Vmiu_yz(i,j,k)+Vmiu_xz(i,
                j,k);
        end
    end
end
xslice = [x(2),x(10),x(16)]; yslice = []; zslice = [];
slice(x,y,z,Vmiu,xslice,yslice,zslice); xlabel('x'); ylabel('y');
    zlabel('z')
shading flat

subplot(1,3,3)
Vmiu = zeros(length(x),length(y),length(z));
for i=1:length(x)
     Vmiu_yz(i,:,:)=miu(N-1,:,:,time3);
    for j=1:length(y)
        Vmiu_xz(:,j,:)=miu(:,N-1,:,time3);
        for k=1:length(z)
```

```
            Vmiu_xy(:,:,k)=miu(:,:,N-1,time3);
            Vmiu(i,j,k)=Vmiu_xy(i,j,k)+Vmiu_yz(i,j,k)+Vmiu_xz(i,
                j,k);
        end
    end
end
xslice = [x(2),x(10),x(16)]; yslice = []; zslice = [];
slice(x,y,z,Vmiu,xslice,yslice,zslice);xlabel('x');ylabel('y');
    zlabel('z')
shading flat
colorbar('eastoutside');
%
    %=====================================================================


figure('DefaultAxesFontSize',12)
subplot(1,3,1)
Vrho = zeros(length(x),length(y),length(z));
for i=1:length(x)
     Vrho_yz(i,:,:)=rho(N-1,:,:,time1);
    for j=1:length(y)
        Vrho_xz(:,j,:)=rho(:,N-1,:,time1);
        for k=1:length(z)
            Vrho_xy(:,:,k)=rho(:,:,N-1,time1);
            Vrho(i,j,k)=Vrho_xy(i,j,k)+Vrho_yz(i,j,k)+Vrho_xz(i,
                j,k);
        end
    end
end
xslice = [x(2),x(10),x(16)]; yslice = []; zslice = [];
slice(x,y,z,Vrho,xslice,yslice,zslice);xlabel('x');ylabel('y');
    zlabel('z')
```

```
shading flat

subplot(1,3,2)
for i=1:length(x)
    Vrho_yz(i,:,:)=rho(N-1,:,:,time2);
   for j=1:length(y)
       Vrho_xz(:,j,:)=rho(:,N-1,:,time2);
       for k=1:length(z)
           Vrho_xy(:,:,k)=rho(:,:,N-1,time2);
           Vrho(i,j,k)=Vrho_xy(i,j,k)+Vrho_yz(i,j,k)+Vrho_xz(i,
              j,k);
       end
   end
end
xslice = [x(2),x(10),x(16)]; yslice = []; zslice = [];
slice(x,y,z,Vrho,xslice,yslice,zslice); xlabel('x'); ylabel('y');
   zlabel('z')
shading flat

subplot(1,3,3)
for i=1:length(x)
    Vrho_yz(i,:,:)=rho(N-1,:,:,time3);
   for j=1:length(y)
       Vrho_xz(:,j,:)=rho(:,N-1,:,time3);
       for k=1:length(z)
           Vrho_xy(:,:,k)=rho(:,:,N-1,time3);
           Vrho(i,j,k)=Vrho_xy(i,j,k)+Vrho_yz(i,j,k)+Vrho_xz(i,
              j,k);
       end
   end
end
xslice = [x(2),x(10),x(16)]; yslice = []; zslice = [];
```

```
slice(x,y,z,Vrho,xslice,yslice,zslice);xlabel('x');ylabel('y');
    zlabel('z')
shading flat
colorbar('eastoutside');
    function f=fminrho(m,r)
        f=P*(m-r)+((Tin*m)./(Sa*(Kin+m))-(Tout*r)./(Sa*(Kout+
            r))); %%%drug exchange btn the ECF and plasma(16)
    end
end
```

RESEARCH OUTPUTS

Publication

Kashaju, N., Kimathi, M., & Masanja, V. G. (2021). Modeling the Effect of Binding Kinetics in Spatial Drug Distribution in the Brain. *Computational and Mathematical Methods in Medicine*, *2021*. https://doi.org/10.1155/2021/5533886

Poster Presentation

Modeling the Effect of Binding Kinetics in Spatial Drug Distribution in the Brain.